Structure and Spin Dynamics in Cr Doped ZnO

by

Paul Erhire Amami

submitted in accordance with the requirements for

the degree of

MASTER OF SCIENCE

In the subject

PHYSICS

at the

UNIVERSITY OF SOUTH AFRICA

SUPERVISOR: PROF. VIJAYA SRINIVASU VALLABHAPURAPU

CO-SUPERVISOR: DR. JAYASHREE DAS

June 2016

Declaration

I declare that Structure and Spin Dynamics in Cr Doped ZnO is my own work and that all sources that have been used or quoted have been indicated and acknowledged by means of complete references.

Signature:..... Date:.....

(P E Amami)

Dedication

I dedicate this work to my beautiful and lovely wife, Helga and my adorable daughter, Bella. Their love, support, encouragement and prayers kept me strong throughout this work.

Acknowledgment

- I would first like to thank my supervisors Prof. V.V. Srinivasu and Dr. Jayashree Das, for giving me this very thought-provoking research project. Their guidance, inspiration and knowledge sharing have been truely invaluable.
- My sincere thanks goes to the Unisa department of Physics for their unwavering support.
- I am indebted to Prof. H. I. Atagana (UNISA) for his support and care.
- To my family, for their utmost belief in me. Their encouragement, love and financial support is priceless. I deeply appreciate and may God bless you all.
- To my beautiful angel, Helga. You are a noble gift and a blessing, for providing me with unfailing support and continuous encouragement throughout my years of study, research and thesis writting. This accomplishment would not have been possible without your support. Thank you.
- Above all, I am humbled and overwhelmed with God's love, blessings, protection and guidance in the course of this work and my entire life.

List of figures

List of tables

Abstract

Polycrystalline $Zn_{1-x}Cr_xO$ ($0.01 \leq x \leq 0.09$) samples synthesized by solid state reaction technique were sintered at different temperatures following slow step sintering schedule. Structural, micro-structural, optical, magnetic properties and homogeneity were investigated using suitable characterisation techniques. Cr_2O_3 and CrO_2 phases have been detected in the XRD patterns and Raman spectra of $Zn_{1-x}Cr_xO$ samples with $x \geq 0.05$. Photoluminescence study has indicated improved optical property of the samples compared to undoped ZnO. While low percentage Cr doped samples showed diamagnetic behaviour, higher percentage doped samples ($\geq$ 5%) exhibited ferromagnetic, paramagnetic and anti-ferromagnetic behaviours depending upon the sintering temperatures. The magnetic properties have been analysed through Electron Spin Resonance study. A g-value of 1.97 indicates Cr in +3 valence state in doped ZnO system. Presence of Cr^{3+} and Cr^{4+} in ZnO is understood to facilitate super exchange interactions to promote ferromagnetism at room temperature. ESR study shows improved magnetic homogeneity achieved by slow step sintering process.

Keywords: Semiconductors; Magnetic properties; Raman Spectroscopy; X-ray diffraction; Electronic paramagnetic resonance; Photoluminescence Spectroscopy; Ferromagnetism; Diluted Magnetic Semiconductors, Anti-ferromagnetism; Paramagnetism.

Table of Content

CHAPTER ONE

1.0 Introduction

Starting from the Stone Age in the ancient civilization through medieval technologies to the industrial revolution in the $19^{th}$and 20^{th} century, materials have played a pivotal role in human advancement. As we enter into the new millennium, high value added advanced materials in form of metals, alloys, ceramics and composites are in the forefront to solve current problems faced in the world. Research on quantum computers, nanotechnology, bioengineering, nuclear fusion, advanced materials, superconductivity, alternative fuels, LEDs and solar cells are on the forefront to solve problems like energy crisis, pollution and environmental safety [1-3]. In space science, similar developments are also observed in spacecraft designing and space missions. Where application of materials has been our ultimate goal, a firm theoretical basis is needed for its efficient implementation, giving attention to understand materials' behavior from the atomic level using various advanced analytical techniques. Among all the materials, semiconductors could find a very important place owing to its tremendous application in communication, computer industry and information technology. All long recent half of the century, miniaturization of semiconductor devices has hold a major focal point in society to increase integration, increase functionality, and cut down energy usage. Apart from the conventional elemental semiconductors like Si and Ge, there are compound semiconductors which are composed of elements from two or more different groups of the periodic table, the prominent members being GaAs, InGaAs, GaN, ZnO, TiO_2, and SnO_2 etc. Nevertheless, for high frequency, high voltage, high temperature, sensor applications and high power devices, semiconductors with wide band gap like Zinc

oxide and Gallium nitrides hold amount of virtue that are of various orders of magnitude higher compared with typical semiconductors [4,5].

Recently it has been suggested that increased spin-polarized carrier population might be locally introduced by substituting magnetic ions onto lattice sites of semiconducting hosts of diluted magnetic semiconductors (DMS) [6]. In past few decades, oxide semiconductors such as ZnO, TiO_2, and SnO_2; with blended properties of ferro-electricity, high permittivity, superconductivity, magnetism and photo-electricity, have been used in many application fields. In oxide electronics, it is possible to combine all these excellent properties in the monolithic configuration to design the hyper-intelligent devices. However, to realize optical spintronics devices such as light emitting diodes (LED), optical isolators and quantum computers, it is very important that these oxide semiconducting materials should also have magnetism with high Curie temperature (T_C) along with good optical (luminescence) properties. In this regard, ZnO has become popular as a promising candidate for the realization of near- or above-room temperature ferromagnetism by doping with transition metals in addition to good optical properties [7, 14].

1.1 Semiconductors

Materials with electrical resistivity that intermediate with those of insulators and conductors are referred to as semiconductors. These materials are very important in today's electronics. Their electrical properties are as a result of very small concentrations of impurities. They are known as narrow band gap insulators. The band gap of semiconductors is much smaller than insulators, between the top of the highest filled band known as the valence band. The bottom of the vacant band just above the valence band is known as the conduction

band as shown in figure 1.1. The energy gap between the conduction and valence band is in the order of 1eV at room temperature.

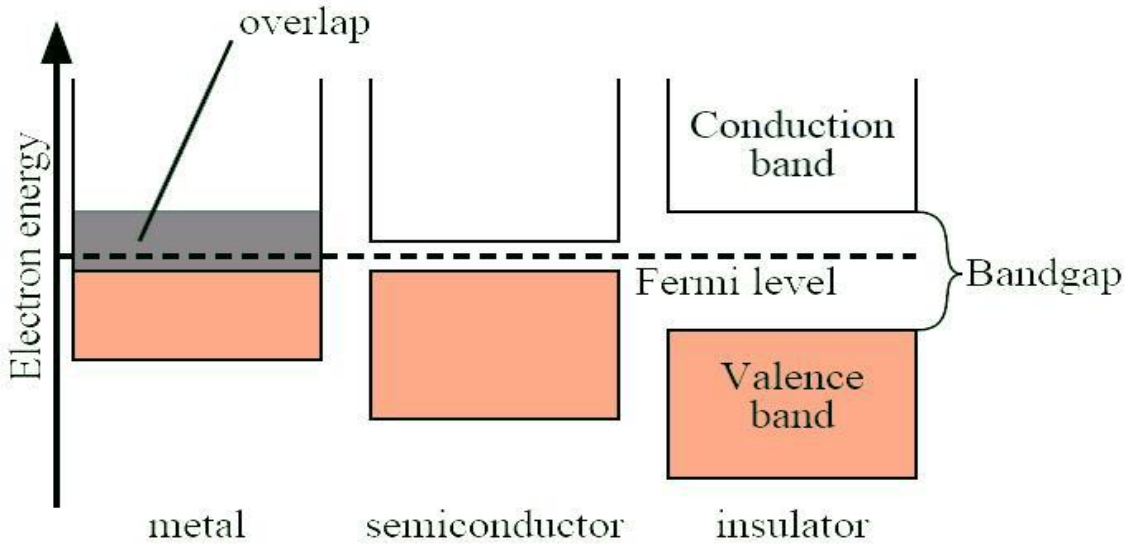

Figure 1.1 Schematic diagram of band gap difference in metal, semiconductor and insulator [23].

1.3 Background of the study

Today's miniaturization in information technology requires semiconductivity and magnetism together in a device which could perform both spin and charge, to process and store data. The combination of spin and charge properties enables powerful, integrated multifunction computing systems in the domain known as spintronics. Unique applications like chip-based memory that are nonvolatile, reconfigurable logic, and nonvolatile Magnetic Random Access Memory (MRAM), spin-polarized LEDs and Spin Field Effect Transistor are possible with these magnetic semiconductor systems [8, 9]. The initial discovery paving way to these advancement, the discovery of giant magnetoresistance (GMR) in magnetic multilayered materials, early economic spintronic giant magnetoresistance based devices, as

well as giant magnetoresistance sensors and hard drives of high-capacity, became accessible in late 1990's and are today the current technology for data read-out in hard drives. For valid practical applications, it is indispensable for the spin polarized carriers to hold a stable source and transport these spin polarized carriers inside the device [10]. Hence, the system must hold a ferromagnetic material to support long storage of the electron spins and the system must also have a semiconductor segment, over which conventional device operation can function. Relating to this, semiconductors doped with transition metals to give magnetic functionality otherwise referred to as diluted magnetic semiconductors (DMS). They are reported to exhibit excellent result in spintronics technology. Figure 1.2 shows the schematic of DMS.

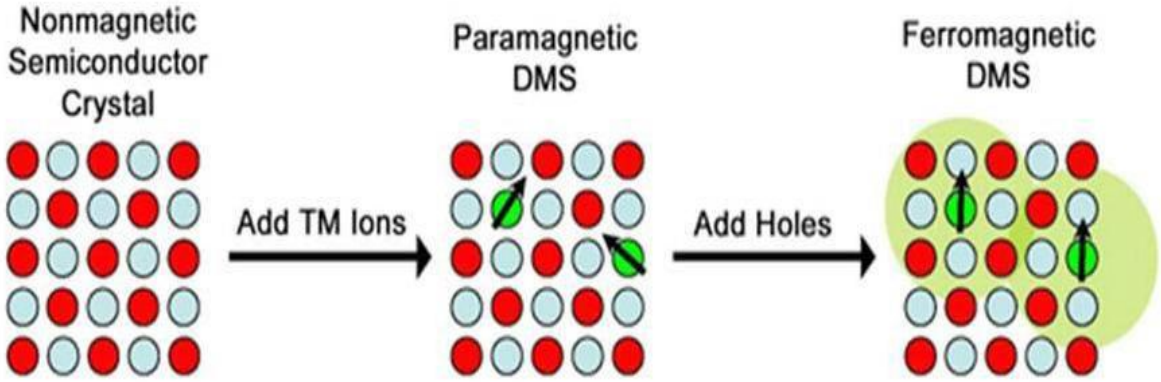

Figure 1.2: Schematic of non-magnetic semiconductor, paramagnetic DMS, ferromagnetic DMS [24]

Their semiconducting property originates from the interaction between 'd' electrons (the localized TM^{2+} ions) and the s and p- like orbital of the band electron, which is known as sp-d exchange interaction [11]. However, researchers currently aim to achieve a DMS, where the electrons have a tunable high grade of spin polarization making it possible to design electronic devices like spin valves, transistors, spins light emitting diodes (SLED), ultra-fast optical switches and non-volatile memories. In addition, it is absolutely necessary for these

diverse applications that the DMS show ferromagnetism at room temperature. The mechanisms of DMS behavior can be understood from several microscopic models proposed so far, like direct exchange interaction, RKKY interaction, super exchange interaction, Bound Magnetic Polarons model etc [12, 13]. Advancement in attaining magnetic ordering at high temperatures in technologically practical semiconductors, include wide band gap nitrides (GaN) and oxides (ZnO) following the theoretical prediction by T. Dietl *et al* as shown in figure 1.3 [14, 15].

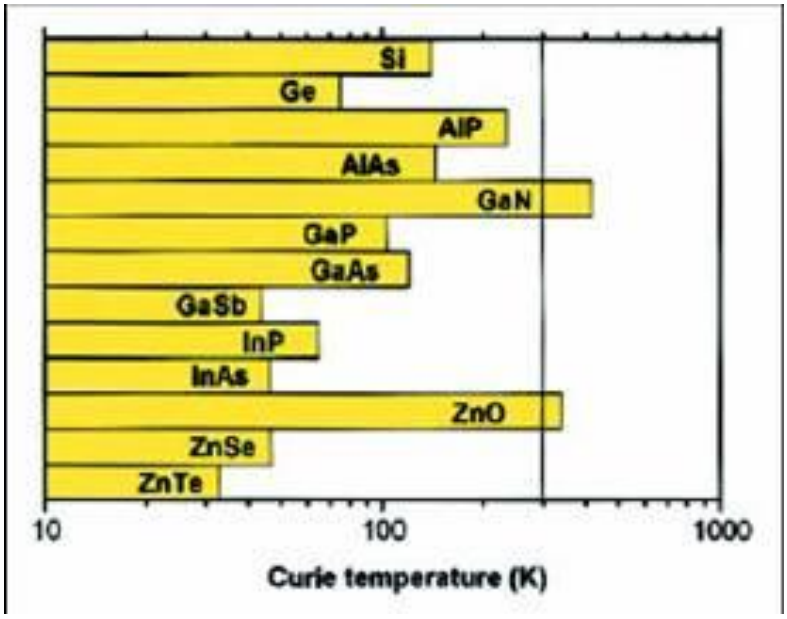

Figure 1.3 Semiconductors with their Curie temperatures (T_C) [14].

However, compared to non-oxide semiconductors, the oxide semiconductors have innumerable advantages, such as wide band gap which cause them to be transparent and applicable for functions with short wavelength. It is also seen to be easily produced at low temperature alike with plastic substrate which are eco-friendly and lifelong, likewise it is cost effective. Apart from these, active electro negativity of oxygen is expected to give an active p-

d exchange coupling between the localized spins and the band carries, which is a prerequisite for DMS. Therefore, oxide based semiconductors exhibit a phenomenal range of optical, electrical and magnetic properties, offering a befitting platform for the convergence of electronics, optics and magnetic behaviors. Under this circumstance, it is highly desirable as well as demanding to search for newer and multifunctional materials with novel characteristics required for better practical applications.

1.4 Research Problem and Research Objectives

As known, in ZnO based DMS, spin dependant magnetic phenomena can be manipulated by the addition of small amount of magnetic impurities like 3d transition or 4f rare earth metal atoms. The unpaired 'd' or 'f' electrons of the dopant ions would give rise to a magnetic moment. Transition metal dopants such as Mn, Cu, Ni, Co or Fe can easily enter the host semiconductor, due to their high solubility and diffusivity without precipitation as secondary phases or metallic nanoclusters. After the first room temperature ferromagnetism in Co doped ZnO films reported by Ueda et al.,[17] many significant experiments were carried out by many researchers which showed a broad range of magnetic behavior and in their anticipated origin for TM (Co, Fe, Ni and Mn) doped ZnO systems prepared by different techniques. RTFM observed in these systems mainly depended on optimization of processing parameter such as doping concentration and conditions. The exact role of optimizing processing parameters and the effect of TM doping in ZnO reqiures further investigation. This is important for enheancing of electrical, optical and magnetic properties of TM doped ZnO. One of the problems associated with ZnO is the dependence of the properties on the synthesis technique [16 -19].

For successful injection of spin polarized carriers and true practical application, it is

important to have a stable and reproducible ferromagnetic phase at room temperature. This is not easy to achieve in ZnO. The room temperature ferromagnetism (RTFM) nature needs to be intrinsic in origin and not due to impurity phase or TM magnetic clusters [19]. Defects like oxygen vacancies are known to affect the magnetic properties of pure undoped and doped ZnO. The magnetic behavior in TM doped ZnO also depends on the choice of dopant, dopant concentration and optimization, substrate choice, processing temperature etc [19].

The objective of the study is to study magnetic, electron spin resonance and optical properties of Cr doped ZnO system. In order to resolve these problems, polycrystalline bulk samples of TM (Cr) doped ZnO will be prepared by using highly pure starting material (99.999% purity) to avoid the possibility of any contamination. The samples will be sintered by a unique and novel slow step sintering technique, to have a single phase stable structure [20]. The ferromagnetic state of Cr doped ZnO had been identified as more stable and energetically favorable [21, 22].

1.5 Summary of this thesis

This thesis is outline as follows. Literature review on the related works on ZnO is given in chapter two. In chapter three experimental details are given. Results and discussions are presented in chapter four and conclusions are in chapter five.

1.6 References

[1] Energy and Transportation: By National Research Council, Publisher: National Academies Press, (2003) p. 4-7.

[2] Minoru Taya, Electronic Composites, Cambridge university Press, (2005) p. 1-3.

[3] W. D. Callister, Jr., Materials Science and Engineering, 6th edition, John Wiley, (2004), p. 77.

[4] T. Fukumura, Y. Yamada, H. Toyosaki, T. Hasegawa, H. Koinuma, M. Kawasaki, Cond-mat, (2003) 0305435.

[5] Anderson. Janotti and C. G Van de Walle, Rep. Prog. Phys. **72** (2009) 126501 (29pp).

[6] R. N. Gurzhi, A.N. Kalinenko, A.I. Kopeliovich, A.V. Yanousky, E.N. Bogachek, U. Landman, Phys. Rev. B 68 (2003) 125113.

[7] R. Janisch, P. Gopal, N. A. Spaldin, J. Phys. Condens. Matter 17 (2005) R657e89.

[8] S.A. Wolf, et al., Science, 294 (2001) 1488.

[9] S. Das Sarma, J. Fabian, X. Zu, I. Zutic, Superlattices and Micr ostructures, 27 (5/6), (2000) 289.

[10] G. A. Prinz, Science 282 (1998) 1660.

[11] R. R. Galazka: Proc. 14th Int. Conf. Physics of Semiconductors, Edinburgh, (1978) 133.

[12] R. Janisch, P. Gopal and Nicola. A Spaldin, J. Phys.: Condens. Matter 17 (2005) R657–R689.

[13] J. M. D. Coey, M. Venkatesan, and C. B. Fitzgerald, Nature Materials, 4, (2005) 173 – 179.

[14] T. Dietl, H. Ohno, F. Matsukura, J. Cibert, and D. Ferrand, Science **287** (2000) 1019-1022.

[15] S. J Pearton, D.P Norton, M.P. Ivill, A.F. Hebard, J.M. Zavada, W.M. Chen, I.A. Buyanova, Journal of Electronic Materials (2007) 462–471.

[16] U. Ozgur et al., A comprehensive review of ZnO materials and devices**,** Appl. Phys. 98, 041301 (2005) 68-76.

[17] Ueda K, Tabata H, Kawai T, Appl. Phys. Lett. 79, (2001) 988.

[18] C. Liu, F. Yun, H. Morkoc¸ Journal of Materials Science: Materials in Electronics 16 (2005) 555– 597.

[19] F. Pan, C. Song, X.J. Liu, Y.C. Yang, F. Zeng, Materials Science and Engineering R62 (2008) 1–35.

[20] J. Das, S.K. Pradhan, D.R. Sahu, D.K. Mishra, S.N. Sarangi, B.B. Nayak, S. Verma, B.K. Roul, Physica B 405 (2010) 2492–2497.

[21] X. Pang, J. Zhang, K. Gao, A.A Volinsky, Materials Letters 65 (2011) 2728–2730.

[22] K. Sato, H. Katayama-Yoshida, Semicond. Sci. Technol. 17 (2002) 367.

[23] http://analyseameter.com/2016/02/semiconductor-electronics-basic-theory.html (Accessed 20th January 2016).

[24] https://www-als.lbl.gov/index.php/science-highlights/science-highlights/230-electronic-structure-and-magnetism-in-diluted-magnetic-semiconductors.html (Accessed 20th January 2016).

[25] G. Z. Xing, J. B. Yi, D. D. Wang, L. Liao, T. Yu, Z. X. Shen, C. H. A. Huan, T. C. Sum, J.Ding, T. Wu, Physical Review B 79, (2009) 174406, 1-9.

CHAPTER TWO

Literature Survey

2.1 Importance of ZnO

Zinc oxide (ZnO) is an n-type semiconductor with wonderful properties which includes magnetic, optical, and piezoelectric properties. It thus has a wide range of applications in transparent electronic, optoelectronic, spintronics, gas and chemical sensors [1]. Vast industrialized benefits of ZnO comes from its ecofriendly nature, wide sufficient sources and low costs of metal Zn [1]. Semiconductor Zinc oxide has attained sufficient importance in the research society partly due its large exciton binding energy of 60 *me*V and its direct wide band gap of 3.37eV at room temperature [2, 3] that can point to lasing action established on exciton recombination, possibly above room temperature. Also it can be used for dynamic exciton based emitters at room temperature and acute growth promoting very small brick semiconductor lasers. The research focusing on ZnO has been going on for many years. The room temperature ferromagnetism of transition metal doped DMS is still in dispute [1, 4]. A wide range of industrial applications of ZnO are its band gap which is near ultraviolet, piezoelectric and optoelectronic properties [6]. The difficulty in fabricating low resistivity and reproducible p-type ZnO has hindered its potential applications in electronic industry. The room temperature ferromagnetic (RTFM) property and its origin in ZnO is not yet understood [6].

2.2 Structure and Physical Parameter of ZnO

In figure 2.1 we show the crystal structure of ZnO. It crystallizes Zinc oxide with wurtzite hexagonal structure, B4 space group, which can exist in B1, cubic rocksalt structure and B2,

hexagonal zinc-blende structure. The latter two not thermodynamically stable in bulk samples [5]. Only the zinc oxide B4 wurtzite structure is thermodynamically stable in bulk samples[4].

It belongs to the space group $P6_3mc$ and has two interrelated sublattices of Zn^{2+} and O^{2-}. The Zn ion is ringed around with a tetrahedral coordination of O ions. The wurtzite structure of zinc oxide has surface structure of polar Zn terminated (0001), O terminated $(000\bar{1})$ which are c-axis aligned and non-polar $(11\bar{2}0)$ and $(10\bar{1}0)$ surfaces. These surfaces have different physical and chemical properties. The electronic structure of O terminated $(000\bar{1})$ surface is marginally different from the three other surfaces. This $(10\bar{1}0)$ and polar surfaces are known to be stable while $(11\bar{2}0)$ is found to be less stable. The sp^3 covalent bonding in ZnO is a result of the tetrahedral coordination [6].

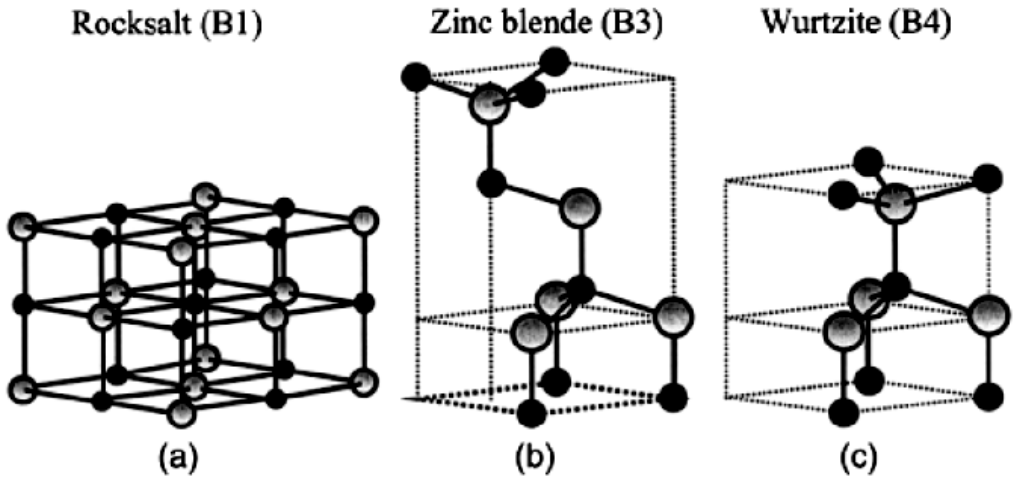

Figure 2.1: The crystal structures of ZnO. ZnO crystallizes in (a) B1, cubic rocksalt structure, (b) B3, hexagonal zinc blende structure, (c) B4, $P6_3mc$ wurtzite.

A semiconductor lattice parameter, generally rely on the following factors: (i) free-electron concentration, (ii) temperature, and (iii) external strains [4, 7]. To accurately measure

the lattice parameters of any semiconductor, high resolution X-ray diffraction (HRXRD) by using a set of symmetrical and asymmetrical reflections of the Bond method is used [8]. The lattice parameter of ZnO wurtzite structure is given as, a = 3.29 Å, c = 5.29 Å [4, 9]. Different theoretical calculations and experimental measurements of lattice constants for zinc wurtzite structure at room temperature are in concession with one another. It is reported from literature that Zn-O bond length is approximately 0.198 nm and may change slightly due to incorporation of dopants in undoped ZnO lattice [10]. The impurities introduced to ZnO results in changes in bond length of Zn-O and also a change in the bond angles [11]. For ZnO to be successfully used for device applications, it is important to take the band structure into consideration which helps to predict the electrical properties. ZnO wurtzite band structure has been calculated from different theoretical and experimental approach. Its electronic levels have been conventionally measured using UV emission/absorption or X-ray techniques which essentially measures the energy difference. The photoelectric effect in the X-ray region apparently can also be used to study the energy region and also angle-resolved photoelectron spectroscopy. Some of the most commonly used computational methods used in studying the band structure of zinc oxide are the density functional theory (DFT) and local density approximation (LDA). To explain the Zn 3*d* electrons the local density approximation (LDA) and incorporating atomic self-interaction corrected pseudo potentials (SIC-PP) have been used (see figure 2.2). The high symmetry lines in the hexagonal Brillouin shows the band structure. An optical band gap of about 3.3eV is in between the occupied band which shows the energy difference [6, 12, 13].

ZnO has gained much attraction in the research community due to its physical parameters as a transparent semiconductor for optoelectronic applications such as light emitting diode (LED), photodetectors, lasers and piezoelectrical applications [4]. It is important to understand the

physical properties of ZnO in other to produce conventional devices. Physical properties of ZnO are highlighted in the table 2.1.

Table 2.1: Physical properties of ZnO [14].

Property	Value
Lattice parameters at 300 K	a_o = 0.32495 nm c_o = 0.52069 nm a_o/c_o = 1.602 (1.633 for ideal hexagonal structure)
u	0.345
Density	5.606 g/cm^3
Stable phase at 300 K	wurtzite
Melting point	1975^o C
Thermal conductivity	0.6, 1-1.2
Linear expansion coefficient (/^{o}C)	a: 6.5 x 10^{-6}, c; 3.0 x 10^{-6}
Static dielectric constant	8.656
Refractive index	2.008, 2.029
Energy gap	3.4 *e*V (direct)
Intrinsic carrier concentration	<10^6/cm^3
Exciton binding energy	60 *me*V
Electron effective mass	0.24
Electron Hall mobility T 300 K for low *n*-type conductivity	200 cm^2/V.s
Hole effective mass	0.59
Hole Hall mobility at 300 K for low *p*-type conductivity	5-50cm/V.s

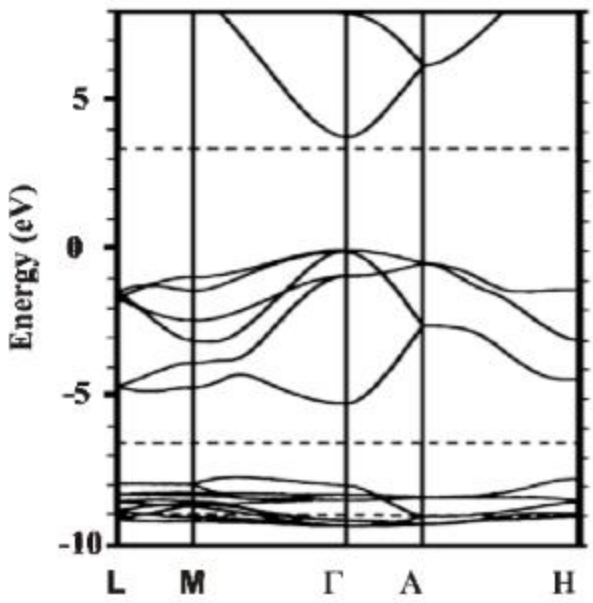

Figure 2.2: ZnO wurtzite band structure calculated using local density approximation (LDA) and incorporating atomic self-interaction corrected pseudo potentials (SIC-PP) [6].

2.3 Electrical properties of ZnO

ZnO is a multifunctional material due to its large band gap making it a material for electronic and optoelectronic applications and exhibits defect or impurity dominated conductivity. It has inevitable existence of electrically active native defects and impurities consisting of donor ionization energies [17,18,114]. Because of its large band gap it is able to retain high temperature and high power operation, higher voltage breakdown and also able to sustains large electric fields. ZnO is an n-type semiconductor even without intentional doping and still remains controversial. Lack of p-type has hinder its use in device application. The anisotropy of ZnO wurtzite structure facilitates the electrical properties of ZnO [115]. One of the techniques used in low-field transport to measure electrical properties is the Hall Effect which can also tell more about the condition of the epitaxial layers. In a wide range of

temperature of 4.2- 300 K the Hall measurements can give detail information on uniformity, impurities imperfection, etc. [17,18]. It is believed that oxygen and zinc interstitials native defects are responsible for the electrical properties of ZnO and its conductivity increase with temperature. The carrier concentration of undoped ZnO is as low as 10^{15} cm^{-3} while in doped ZnO its carrier concentration is about 10^{20} cm^{-3}. High resistivity of $>10^{8}$ Ωcm is needed for piezoelectric devices and this is attainable by doping of ZnO, however attaining high conductivity for ZnO p-type has proved to be difficult [15, 16]. The carrier densities also affect the electrical conductivity which is as a function of the Fermi energy level.

2.4 Optical Properties of ZnO

The basis of most optoelectronic devices such as light-emitting diodes, lasers, photodetectors lies on the extrinsic and intrinsic effects of optical properties of the semiconductor [19 - 21] and as mentioned earlier, ZnO has gained significant attention in the research community dues its room temperature large binding exciton energy of 60 *me*V and direct wide band gap of 3.37eV [22 - 24].

The optical absorption is influenced by the electronic states created in the bandgap related to point defects or dopants which gives the extrinsic properties and the intrinsic property is as a result of holes in the valance band and electrons in the conduction band [20, 21, 25]. The optical properties of ZnO is investigated using the luminescence technique [26]. Despite the growth method for ZnO, it shows two luminescence bands, a short wavelength band and a long wavelength band [27]. The short wavelength band is located near the absorption edge while the long wavelength is at maximum in the green spectral region [27, 28]. However, the extrinsic luminescence and intrinsic luminescence is still controversial. Undoped ZnO photoluminescence spectrum at low temperature usually contains sharp excitonic lines in the ultra-violet region and in the visible region showing one or more broad

band. At room temperature, these broad bands of green, red, yellow and orange have been observed but it is still unsubstantiated even from many recent report. Oxygen vacancies V_O, oxygen interstitials O_i and zinc vacancies V_{Zn}, are attributed to these bands [4, 29-31].

The optical and electrical properties of ZnO can be greatly affected by native defects which affect luminescence efficiency. Native defect is seen to play a very significant role in zinc oxide and it is believed to display great unintentional n-type conductivity which is seen to be caused by zinc interstitials [32, 33]. In ZnO, the native shallow donor is indicated to be zinc interstitials and the deep donor is of the oxygen vacancies [34, 35]. The green emission observed in ZnO is as a result of single ionized vacancies in zinc oxide and the red luminescence is as result of double ionized oxygen vacancies. Zinc interstitials has higher formation energy than oxygen vacancy [36, 37].

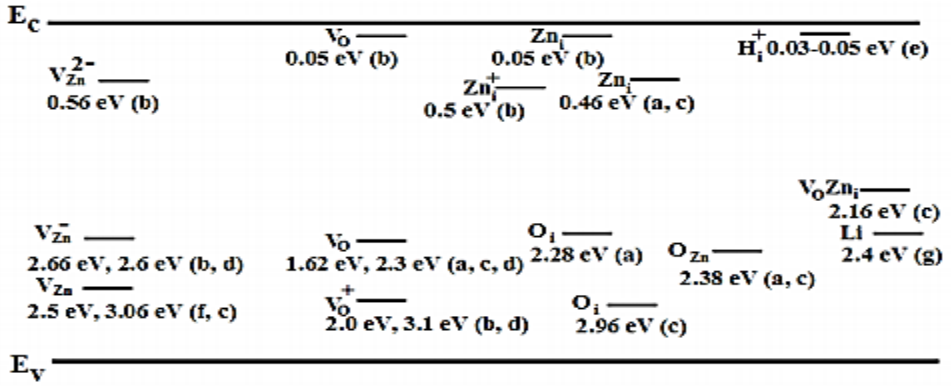

Figure 2.3: Energy levels of the different deep level defects in ZnO [38].

The band emission visible spectrum from 400 nm to 700 nm is usually referred to as deep level emission known as DLE. The energies of 2.4-2.5 eV is seen to where the green luminescence band in zinc oxide is observed. Literature shows that various experimental setups with various samples are still debating the origin of the deep level emission band [38].

At 2.2 eV the yellow emission band is seen to appear [38, 39] and this yellow emission band is a facet to oxygen interstitials as a native defect in Zinc oxide [38].

2.5 Vibrational Properties of ZnO

The vibrational properties of ZnO needs to be understood for effective use in device applications like the resonators. This vibrational property can be studied using suitable techniques like the Raman scattering which can give information about the texture composition, strain and size. Zinc oxide belongs to the C_{6v} symmetry group [17]. According to the group theory, the optical phonons is expressed as

$$\Gamma_{opt} = 1A_1 + 2B_1 + 1E_1 + 2E_2 \qquad 2.1$$

A_1 and E_1 are polar which separates into TO and LO phonons and they Raman and IR active [41, 42]. It has E_2(low), E_2(high), A_1(TO), A_1(LO), E_1(TO) and E_1(LO) Raman active phonon modes, the B_1 modes are silent [17]. The E_2(high) peaks observed usually at 437-439 cm^{-1}, is the characteristic peak of wurtzite ZnO and associated with oxygen displacement, where A_1(LO) peaks located around 570-590 cm^{-1} has been identified as a defect induced mode such as oxygen vacancy, Zn interstitials and other combination due to strong dependence on oxygen stoichiometry [106]. Shuxia Guo *et al* reported that "The Raman mode at about 580 cm^{-1} has been observed by many groups who studied the phonon properties of ZnO-based materials, such as ZnO nanostructures and intentionally doped ZnO samples" [40].

2.6 Defects in ZnO

ZnO has a simple chemical formula with very rich defect chemistry. Oxygen vacancy (V_O), zinc vacancy (V_{Zn}), zinc interstitial (Zn_i) and oxygen antisites (OZn) which are the native defects in zinc oxide play a very significant role in the optical and magnetic properties of pure zinc oxide and doped ZnO. These defects may control doping and minority carrier life

time [32, 43, 47] and determine the properties and performance of ZnO system. In ZnO the V_O vacancy, Zn_i interstitial and Zn anti-site, are donor-type defects while the V_{Zn} vacancy, O_I interstitial, and O anti-site are acceptor-type defects. The O vacancies are deep donors, Zn interstitials are too mobile to be stable at room temperature and a *g*-factor of approximately 1.96 with high deformation energies. Both Zn interstitials and oxygen vacancies donate two electrons [44, 45, 48]. In figure 2.4 and 2.5 we have shown the ZnO native defects with enegy levels and Oxygen Vacancy in ZnO showing its electronic states. The FM coupling between TM ions is mediated via clusters of oxygen vacancies to favour the exchange interaction and long range ferromagnetic ordering at high Curie temperature. Oxygen vacancy can be predicted by Electron paramagnetic resonance measurements (g-value) [46].

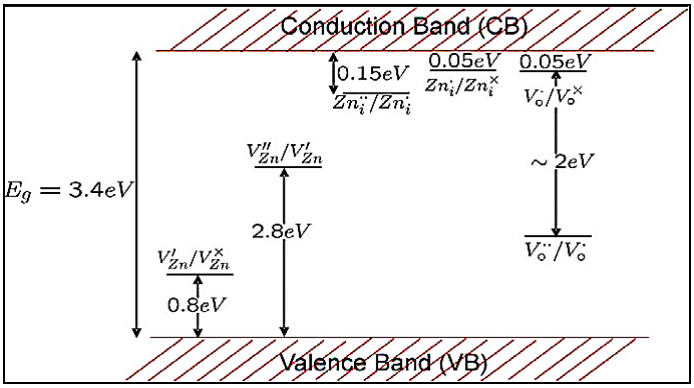

Figure 2.4: ZnO native defects with energy levels [47]

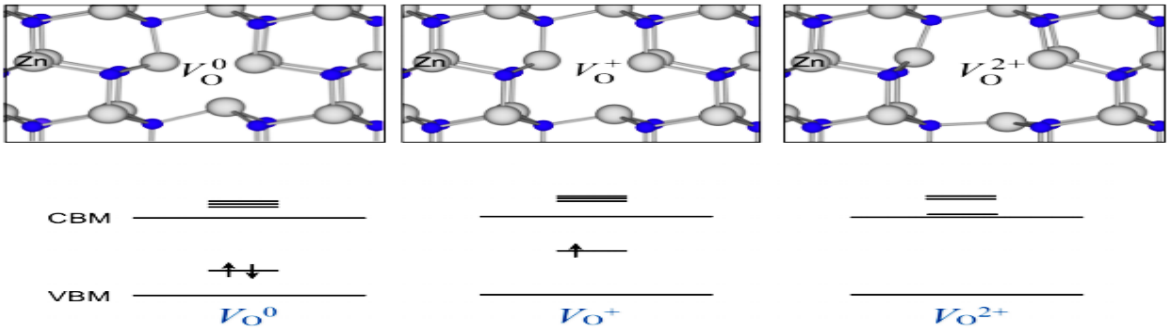

Figure 2.5: Oxygen Vacancy in ZnO showing electronic states [44].

2.7 Doping in ZnO

ZnO occurs as an n-type semiconductor and a possible material for device with short wavelength. Due to the intrinsic defect nature of pure zinc oxide it has very high electron densities. The unintentional doped ZnO is known experimentally as n-type but is still controversial if the donor defects are Zn interstitials and oxygen vacancies. Despite Zn_i and Vo being donors in ZnO, it has been said that hydrogen is a donor that is ionized and has low formation energies. The Group III elements such as Ga, In and Al can also substitute Zn sites with concentration as high as $>10^{20}$ cm^{-3}. Elements such as F, I and Cl in Group VII elements are also known as donors in ZnO. Ge, C, and Si in Group IV could be donor or acceptor impurities but no proof has been shown in this regard [4, 49]. Some groups have report on n-type ZnO doping, S. Kuprenaite *et al* [50], reported In, Ga, and Al-doped ZnO films grown by aerosol-assisted MOCVD with low resistivity of 6.44×10^{-3} Ω cm, 8.16×10^{-4} Ω cm, 7.57×10^{-4} Ω cm respectively. Chaoting Zhu *et al* [51] also reported low resistivity of 3.8×10^{-4} Ω cm for Ga doped ZnO grown using glass substrates by radio frequency magnetron sputtering.

The p-type doping has proven to be more difficult than the n-type doping. This difficulty is attributed to low energy native defects or background impurities. The Group I and Group V elements such as N, P and As are potential dopant candidates for achieving p-type doping of ZnO. The Group I elements can substitute the Zn while the Group V can substitute the O sites. p-type material has been obtained from doping ZnO with N as a shallow donor but the p-type nature appears to be weak having small hole mobilities and Hall voltages [4, 49]. T, K Pathak *et al* [52] reported N doped ZnO thin films grown by the sol–gel and spin coating method showing minimum resistivity of 1.64 Ω cm and carrier concentration of 8.36×10^{17} cm^{-3} with a p-type behavior.

2.8 ZnO-based Diluted Magnetic Semiconductors

Diluted magnetic semiconductor (DMS) is usually a semiconductor doped with magnetic elements like the transition metals (TM) such as Cr, Fe, Co, Mn, Ni, Sc, Ti and rare earth metals (Gd, Dm, Dy, etc). Here a fraction of the host cations can be substitutionally replaced by magnetic ions or appropriate rare earths [53, 54] to give exotic magnetic properties. DMS are potential candidate for spintronic devices which exploit both spin and charge degrees of freedom of the electrons. However, for practical use of DMS material the curie temperature must be at room temperature or just above room temperature [55, 56]. Technologically semiconductors like the wide band gap nitrides (GaN) and oxides (ZnO) are prominent in the research community due to their advancement in attaining magnetic ordering at high temperatures [57, 58]. Since the theoretical prediction by T. Dietl et al for ferromagnetic ordering above room temperature for practical application of spintronic devices, ZnO has been highlighted among research group as a high curie temperature ferromagnetic DMS candidate [53].

Due to Zinc oxide open structure with closed packed lattice Zn atoms occupy half of the tetrahedral sites. The empty octahedral sites provide plenty of sites to accommodate intrinsic defects and extrinsic dopants [58]. In the local density approximation [59], it is predicted that 3d-transition metal (TM) atoms of V, Cr, Fe, Co and Ni show ferromagnetic ordering of their magnetic moments in ZnO without any additional carrier doping treatment [60,61]. The multiple structures observed in d-d optical absorption spectra is due to strong Coulomb interaction between the 3d electrons [62]. On the other hand, the magnetic interaction between the localized 3d spins and the carriers in the host valence band is due to the hybridization between the transition-metal 3d and the host valence band [63]. Besides, ZnO itself can radiate near-ultraviolet light owing to its direct band gap structure and

formation of the stable exciton state [64]. The effect of recombination radiation in the UV region in ZnO can be eliminated by doping ZnO with transition metal ions [65].

However, it has often been observed that dopant materials in ZnO segregate forming precipitates or clusters that seems to be responsible for the ferromagnetic properties. The effect of such ferromagnetic clusters is required to be examined carefully before selecting such materials for spintronics applications [66]. Besides, cause of ferromagnetism in doped oxide materials has been still controversial [67] with several proposed mechanisms like double exchange interaction [68], carrier-mediated Ruderman–Kittel–Kasuya–Yosida (RKKY) type coupling [57], super exchange interaction [57] and F-center exchange interaction [69].

Adequate injection of spin polarized carriers and to construct thin magnetic materials for spintronic devices can be achieved by appropriate doping [4, 54, 66, 70-74]. In order to have suitable material for spintronic device, the DMS material should satisfy the condition that its intrinsic ferromagnetism be maintained at room temperature for functional device design [4]. ZnO doped with TM ions observed to satisfy this condition [28, 75]. Wurtzite ZnO is formed by the tetrahedral s-p^3 bonding. The cations of semiconductor are usually substituted by the 3*d* transition metal ions, i.e; the Zn sites in ZnO [53, 76].

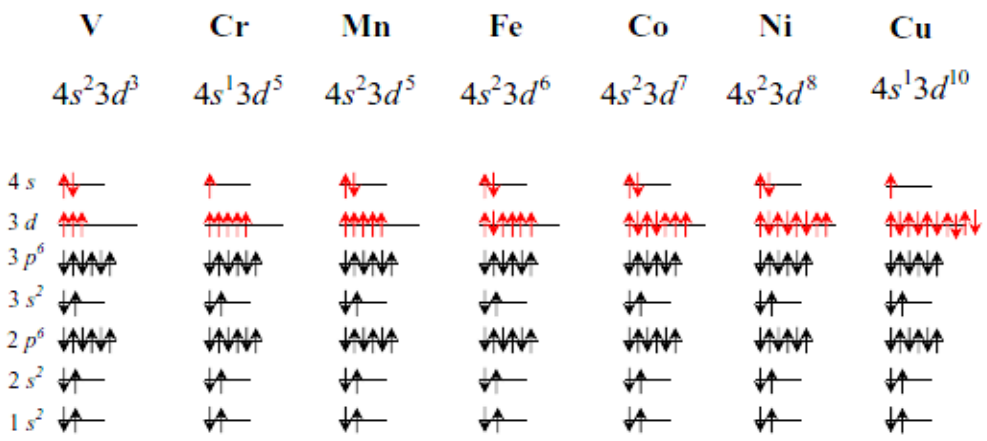

Figure 2.6: Oxidation states and charge states for some transition metal [53, 77]

From different literatures, it is summarised that the issue of ferromagnetic behaviour at room temperature is still controversial in ZnO doped systems [78-82].

Spin-polarized carriers can be introduced by substituting magnetic ions onto lattice sites of semiconducting hosts of diluted magnetic semiconductors (DMS) [104] such as ZnO, TiO_2, and SnO_2. In an oxide semiconductor like ZnO, it is possible to combine the excellent properties of ferro-electricity, high permittivity, superconductivity, magnetism and photo-electricity in the monolithic configuration to design the hyper-intelligent devices. To design spintronics devices such as magnetic random access memories (MRAM), optical isolators and quantum computers, it is strongly desired that these ZnO should have high Curie temperature (T_C) magnetism with good optical (luminescence) properties as well, for which doping with 3d-transition metal (TM) atoms of V, Cr, Fe, Co and Ni [105, 106] have been seen to be beneficial.

However, dopant materials in ZnO frequently segregate forming precipitates or clusters. Also the cause of ferromagnetism in doped oxide materials has been highly controversial. Among the transition metal elements, Cr can be an appropriate dopant as it has close ionic radius to that of Zn, so can substitute Zn position in the crystal [107-109] forming a solid solution. Cr itself is paramagnetic at high temperature and antiferromagnetic below 311 K, hence cannot induce an extrinsic ferromagnetism even if Cr clustering occurs. Again, except CrO_2 which is ferromagnetic; Cr metal, Cr_2O_3, Cr_3O_4 and $ZnCr_2O_4$ are antiferromagnetic nature. CrO_2 has a Curie temperature (T_C) of 386K which is very unlikely to form under low oxygen pressure conditions. Also, the theoretical calculations [110-112] indicate that Cr-doped ZnO should exhibit stable ferromagnetism.

Under this situation, to investigate the Cr doping effect in ZnO, we synthesised, polycrystalline $Zn_{1-x}Cr_xO$ samples by solid state reaction route. All the samples were sintered

by a slow step sintering schedule (SSSS) up to different temperatures [113], which helps in systematic and refined grain growth with stable phase, ensures reproducibility and creates suitable defects/vacancies effectively. All the results pertaining to the experiment and respective analyses are presented and discussed in this report.

In this thesis, we have chosen Cr as our dopant material for ZnO host. Among the transition metal elements, Cr has been an important dopant candidate which has close ionic radius to that of Zn and is expected to easily penetrate into ZnO crystal lattice or substitute Zn position in the crystal [83-85] forming a solid solution. However, the experimental results [83, 85-92] on the studies of Cr doped ZnO are in conflict with each other, although the theoretical calculations [93-95] indicate that Cr-doped ZnO should exhibit stable ferromagnetism [96].

2.9 Mechanism of magnetism in ZnO

The mechanism responsible for magnetism is still not very clear and controversial as mentioned earlier. Different growth method methods in ZnO show different mechanism responsible for their magnetic behaviour. Some of the mechanism that might be responsible for magnetic behaviour in ZnO are highlighted below;

2.9.1 RKKY exchange interaction

The RKKY interaction (Rudermann, Kittel, Kasuya and Yoshida) occurs between magnetic ions and the conduction band electrons mediated by localized spins. Their oscillatory behavior results in no direct overlap around each magnetic electrons and this results in ferromagnetic and antiferromagnetic ordering. The exchange interaction between the localized spin and the *sp* electrons of ZnO is responsible for the ferromagnetism observed at room temperature according to RKKY interaction [97]. Shahid M. Ramaya *et al* [98] in

their report of $Zn_{0.95}Fe_{0.05}Al_xO$ grown with auto-combustion technique observed that the concentration free carriers increase with Al content hence the ferromagnetic behavior is carrier mediated RKKY exchange interactions.

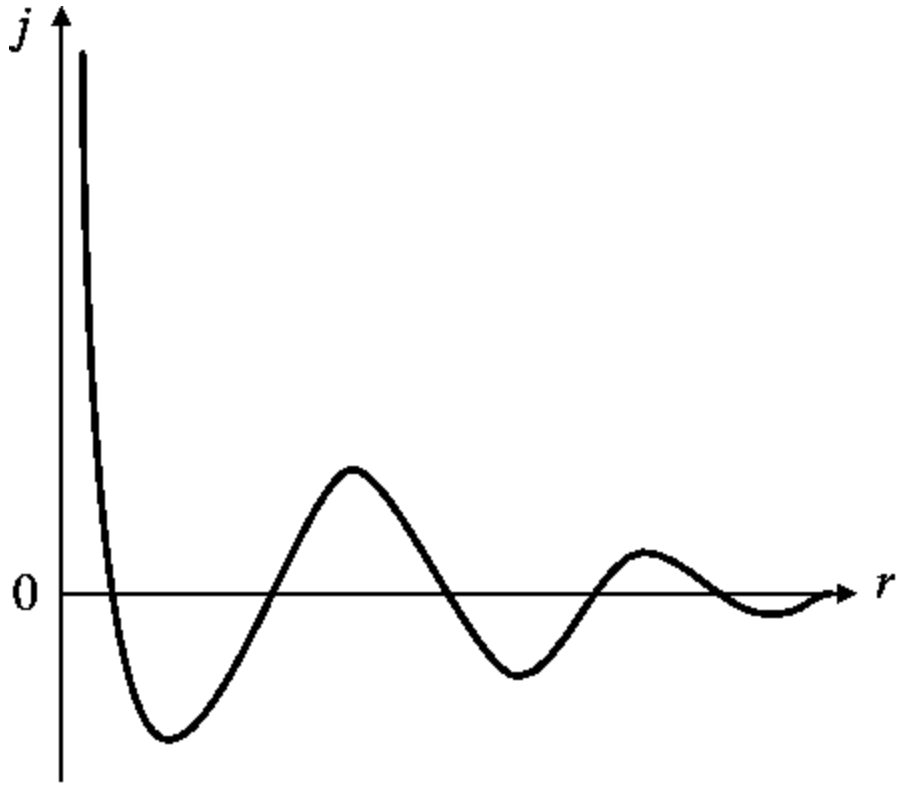

Figure 2.7: RKKY Interaction, where j is the variation of indirect exchange coupling constant of free electron gas in the neighborhood of a point magnetic moment at the origin $r = 0$ (adopted from ref 104)

2.9.2 Superexchange interaction

The superexchange mechanism is a process wherein the spins of two ions are interacting as result of the spin-dependent kinetic exchange interaction between each of the two ions. The spin-spin coupling could either be antiferromagnetic or ferromagnetic. The superexchange coupling distance is short as regards to direct exchange interaction. There is hoping between orbitals usually the localized d-orbitals of transition-metals. Antiferromagnetic coupling is associated with superexchange interaction. The decrease of magnetic moment per Fe atom with increasing Fe concentration appears to be due to

superexchange interaction in Fe-doped ZnO thin films grown by spray pyrolysis technique as reported by A. El Amiri *et al* [98].

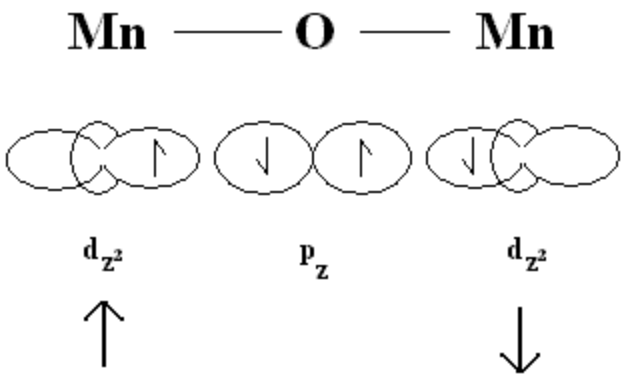

Figure 2.8: Superexchange interactions in MnO systems [105]

2.9.3 Double exchange interaction

This type of exchange interaction is common for systems where the magnetic ion exists in two different valence states usually from the incomplete *d* shells of transition metal. The angle between these two magnetic ions is at 180 degrees and results in ferromagnetic ordering. The double exchange magnetism was first proposed by Zener [100].

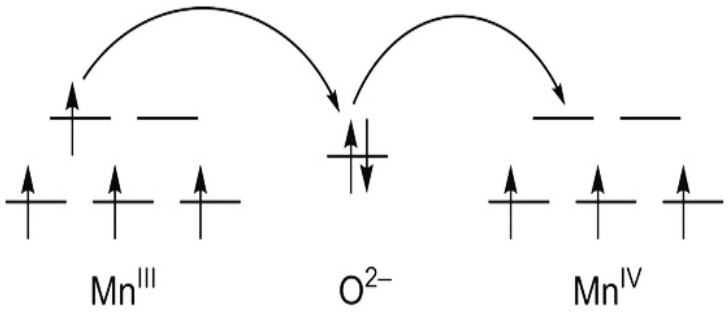

Figure 2.9: Double exchange interaction of Mn-O-Mn

For example, in a Mn doped system the electron that hops from the Mn^{3+} ion should be anti-aligned with the other five electrons on the ion according to Hund's rules (figure 2.5) which

should force out a spin-up electron on the oxygen and hops onto the Mn^{4+} ion. This can only happen which if those electrons are all spin-down.

2.9.4 Bound Magnetic Polarons

In ZnO doped systems the strong exchange interactions between localized spins of transition metal ions and spins of charge carriers is as a result of bound magnetic polarons (BMP). The charge carriers are bounded to the impurities of the polarized spins of the transition metal ions within the bound magnetic polarons thereby reducing the total energy of the system. For doped ZnO systems, the existence of non-ionized acceptors or donors can result in BMPs but these non-ionized acceptors or donors concentration should be comparatively high in order for bound magnetic polarons to be observed. The electrons interact with the spins of the transition metal ions in its orbit thereby resulting in ferromagnetic alignment of the spins [101-103].

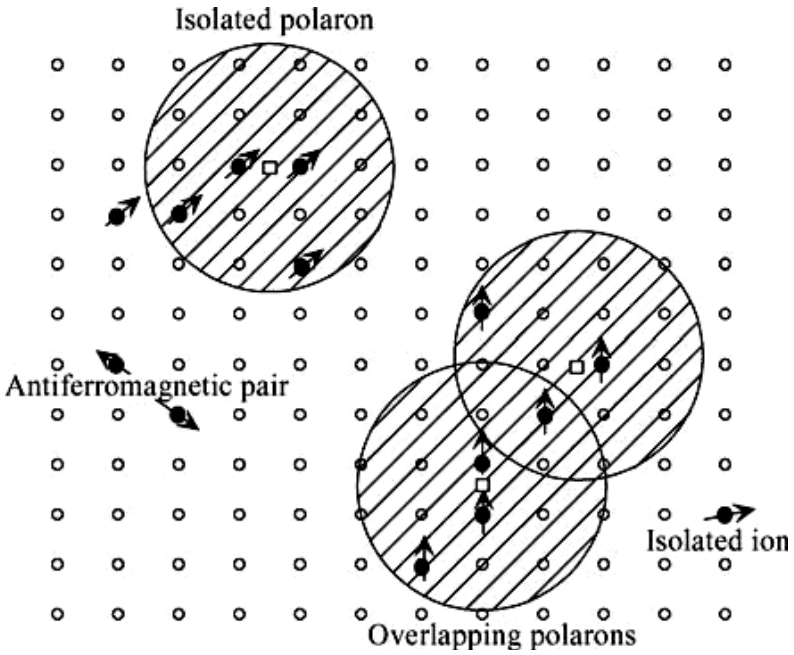

Figure 2.10: Illustration of magnetic polarons [88].

The localized charge carries causes a shift in the insulating state which occurs at a curie temperature lower than the temperature. The interaction distance grows as the temperature decreases. Corresponding clusters of polarons are formed as neighboring polarons overlap and interact due to TM impurities, this happens below the curie temperature. When the size of the sample is equal to the size of the such clusters a ferromagnetic shift is observed. Ferromagnetic ordering may occur from the interaction between BMP due to adequate concentrations of transition metal impurities and antiferromagnetic ordering if the localized holes is from the direct exchange interaction [20].

2.10 Drawbacks / Limitations

One of the limitations and drawbacks of ZnO doped systems is the issue of reproducibility. The magnetic behaviour of DMS materials greatly depends on the synthesis process and hence is not easily reproducible. Also there are no clear indication of the origin of the observed intrinsic ferromagnetism if it as a result of defects such oxygen vacancies or zinc vacancies. The p-type ZnO is still difficult to achieved.

2.11 Our Objective and Plan of work

Under the above mention scenario, we have tried to address the issues mentioned above. We have employed an easy and simple solid state reaction route and a novel slow step sintering schedule (SSSS) to synthesize and process polycrystalline $Zn_{1-x}Cr_xO$ samples. Using highly pure starting material (99.999% purity) to avoid any form of contamination. In order to explain the observed magnetic behavior of DMS materials the Electron Spin resonance techniques have been used which is able to detect magnetic inhomogeneity, spin dynamics, the microscopic structure of the dopant ions and oxygen vacancies.

2.12 References

[1] K. Shtereva, V. Tvarozek, P. Sutta, J. Kovac, and I. Novotny, In Micro Electronic and Mechanical Systems. Vukovar: In-Teh, 2009, p. 211-234.

[2] VD Mote, Y Purushotham ,BN Dole, Journal of Theoretical and Applied Physics, (2012) 6:6.

[3] Look, D.C., Materials Science and Engineering: B, 80, (2001) 381.

[4] U. Ozgur et al., A comprehensive review of ZnO materials and devices**,** Appl. Phys. 98, 041301 (2005) 68-76.

[5] Jasprit Singh, Electronic and Optoelectronic Properties of Semiconductor Structures, Cambridge University Press (2003) p. 10-12.

[6] V. A. Coleman and C. Jagadish., Zinc Oxide Bulk, Thin Films and Nanostructures: Basic Properties and Applications of ZnO, Elsevier Limited(2006) 21-42.

[7] Hakan ÇOLAK, Orhan TÜRKOGLU, Journal of Ceramic Processing Research, (2013) 616-622.

[8] C. Ferrari, E. Buffagni, F. Rossi., Strain and Composition Determination in Semiconductor Heterostructures by High-Resolution X-Ray Diffraction: Characterization of Semiconductor Heterostructures and Nanostructures, Elsevier, (2013) 75-111.

[9] D. R. Lide (Ed.), CRC Handbook of Chemistry and Physics, 73rd Edition, CRC Press, New York, (1992) pp12-40.

[10] A.K. Srivastava, R. Gakhar, P. Dua, K. Senthil, J.S.Tawale, K.N. Sood, K. Yong; Microscopy: Science, Technology, Applications and Education, (2010) 1820-1823.

[11] M. Ghosh, D. Karmakar, S Basu, SN Jha, D Bhattacharyya, SC Gadkari, SK Gupta, Journal of Physics and Chemistry of Solids, 75 (4), (2014), 543-549.

[12] A. Abdelrehim M. Elshaer., Molecular Beam Epitaxy Growth and Characerization of ZnO-based layers and Heterostructures, Cuvillier Verlag (2008), 48-81.

[13] E. Senthil Kumar, Shubra Singh, M. S. Ramachandra Rao, ZnO Nanocrystals and Allied Materials; Zinc Oxide: The Versatile Material an Assortment of Physical Properties, Springer India (2014) 1-38.

[14] D.P. Nortona, Y.W. Heoa, M.P. Ivilla, K. Ipa, S.J. Peartona, , M.F. Chisholmb, T. Steiner; materialstoday, 7, 6, (2004), 34–40.

[15] A. Moezzi, A. M. McDonagh, M. B. Cortie., Chemical Engineering Journal 185–186 (2012) 1–22.

[16] M.D. McCluskey, S.J. Jokela, Defects in ZnO, J. Appl. Phys. (2009) 106.

[17] Cole W. Litton, Donald C. Reynolds and Thomas C. Collins., Zinc Oxide Materials for Electronic and Optoelectronic Device Applications, John Wiley, (2011) 1-131.

[18] Hadis Morkoç and Ümit Özgür., Zinc Oxide Fundamentals, Materials and Device Technology, Wiley-Vch, (2009) 63-70.

[19] D.G. Thomas, J. Phys. Chem. Solids **15**, (1960) 86.

[20] Hadis Morkoç and Ümit Özgür., Fundamentals, Materials and Device Technology, Wiley-Vch, (2009) 131-232.

[21] Zhe Chuan Feng., Handbook of Zinc Oxide and Related Materials: Volume One, Materials, CRC Press, (2013) 167-204.

[22] P. Y. Yu and M. Cardona, Fundamentals of semiconductors: physics and material properties, Springer, Berlin, (2001) 152-202.

[23] Look, D.C., Materials Science and Engineering: B, 80, (2001) 381.

[24] F.K. Shan, Y.S. Yu., Journal of the European Ceramic Society 24 (2004) 1869–1872.

[25] http://encyclopedia2.thefreedictionary.com/semiconductor (Accessed 2nd of March 2016).

[26] Navendu Goswamia, Dhirendra Kumar Sharma., Physica E: Low-dimensional Systems and Nanostructures (2010), 1675–1682.

[27] P.A. Rodnyi, I.V. Khodyuk, Optical and luminescence properties of zinc oxide, Opt. Spectrosc. 111, (2011) 776–785.

[28] B. K. Meyer, H. Alves, D. M. Hofmann, W. Kriegse, D. Forster, F. Bertram, J. Christen, A. Hoffmann, M. StraBburg, M. Dworzak, U Haboeck, A. V. Rodina, Phys. Stat. Sol. (B) (2004), 231-260.

[29] Ching-Ting Lee., Materials (2010), 2218-2259.

[30] K. Vanheusden, C. H. Seager, W. L. Warren, D. R. Tallant, J. A. Voigt., Appl. Phys. Lett. 68 (3), (1996) 403.

[31] N H AlviEmail author, Kamran ul Hasan, Omer Nur, Magnus Willander, Nanoscale Research Letters, (2011) 6:130.

[32] Anderson Janotti and Chris G Van de Walle., Rep. Prog. Phys. **72** (2009) 126501.

[33] Fatma Kayaci, Sesha Vempati, Inci Donmez, Necmi Biyikliab and Tamer Uyar., Nanoscale, (2014), 6, 10224.

[34] S. B Zhang, S. H Wei, A. Zunger., Phys. Rev. B 2001, 63, 075205.

[35] Aleksandra B. Djurisic, Wallace C. H. Choy, Vellaisamy Arul Lenus Roy, Yu Hang Leung, Chung Yin Kwong, Kok Wai Cheah, Tumkur Krishnaswamy Gundu Rao, Wai Kin Chan, Hsian Fei Lui, Charles Surya; Photoluminescence and Electron Paramagnetic Resonance of ZnO Tetrapod Stucture., Adv. Funct. Mater. (2004), 856-864.

[36] N, H Alvi., Luminescence Properties of ZnONanostructures and Their Implementation as White Light Emitting Diodes, Linköping University, Linköping, Sweden, (PhD thesis), 2011.

[37] Fan. Z, Pai-chun Chang, Jia G. Lu, Appl. Phys. Lett. 85, (2004) 6128-6130.

[38] Magnus Willander, Omer Nur, Jamil Rana Sadaf, Muhammad Israr Qadir, Saima Zaman, Ahmed Zainelabdin, Nargis Bano, Ijaz Hussain., Luminescence from Zinc Oxide Nanostructures and Polymers and their Hybrid Devices, Materials (2010), 3, 2643-2667.

[39] Zwingel, D., J. Lumin. 1972, 5, 385–405.

[40] Shuxia Guo, Zuliang Du, Shuxi Dai., Physica Status Solidi (b) Volume 246, Issue 10, pages 2329–2332, (2009).

[41] D.F. Paraguay, M. Miki-Yoshida, J. Morales, J. Solis, L.W. Estrada, Thin Solid Films, 373 (2000), p. 137.

[42] P. Sundara Venkatesh, V. Ramakrishnan, K. Jeganathan., Physica B: Condensed Matter, Volume 481, (2016), Pages 204–208.

[43] Rezq Naji Aljawf, F. Rahman, Shalendra Kumar, Materials Research Bulletin, (2016).

[44] A.Janotti , C. G. Van de Walle, Phys.Rev. B 76, (2007) 165202.

[45] Boris B. Straumal, Andrei A. Mazilkin, Svetlana G. Protasova, Ata A. Myatiev, Petr B. Straumal, Gisela Schütz, Peter A. van Aken, Eberhard Goering, Brigitte Baretzky, Phys. Rev. B 79, (2009) 205206.

[46] J. Das, D.K. Mishra, V.V. Srinivasu, D.R. Sahu, B.K. Roul, Journal of Magnetism and Magnetic Materials 382 (2015) 111–116.

[47] Kröger**,** F. A., The Chemistry of Imperfect Crystals. 2nd Edition, North Holland, Amsterdam (1974), 73.

[48] M. D. McCluskey, S. J. Jokela, J. Appl. Phys. **106**, (2009) 071101.

[49] David C. Look, Zinc Oxide Bulk, Thin Films and Nanostructures, Processing, Properties and Applications: Doping and Defects in ZnO, pp21–42, (2006), Elsevier.

[50] S. Kuprenaite, T. Murauskas, A. Abrutis, V. Kubilius, Z. Saltyte, V. Plausinaitiene, Surface and Coatings Technology, 271, (2015) 156–164.

[51] Chaoting Zhu, Jia Li, Ye Yang, Pinjun Lan, Jinhua Huang, Yuehui Lu, Ruiqin Tan, Ning Dai, Weijie Song, Thin Solid Films, 605, (2016) 95–101.

[52] Trilok Kumar Pathak, Vinod Kumar, H.C. Swart, L.P. Purohit., Physica B: Condensed Matter**,** 480, (2016), 31–35.

[53] C. Liu, F. Yun, H. Morkoc¸ Journal of Materials Science: Materials in Electronics 16 (2005) 555– 597.

[54] F. Pan, C. Song, X.J. Liu, Y.C. Yang, F. Zeng, Materials Science and Engineering R 62 (2008) 1–35.

[55] H. Ohno, Science 281, 5379, (1998) 951-956.

[56] Deng-Lu Hou et al, Xiao-Juan Ye, Huai-Juan Meng, Hong-Juan Zhou, Xiu-Ling Li, Cong-Mian Zhen, Gui-De Tang, Materials Science and Engineering B 138 (2007) 184–188.

[57] T. Dietl, H. Ohno, F. Matsukura, J. Cibert, and D. Ferrand, Science **287** (2000) 1019.

[58] S.J. Pearton, D.P. Norton, M.P. Ivill, A.F. Hebard, J.M. Zavada, W.M. Chen, I.A. Buyanova, J. Electron. Mater. 36 (2007) 462.

[58] S. K. S. Parashar, B. S. Murty, S. Repp3 S. Weber, E. Erdem., J. Appl. Phys. 111, (2012) 113712.

[59] K. Sato, H. Katayama-Yoshida, Jpn. J. Appl. Phys. 39 (2000) L555.

[60] Issei Satoh, Takeshi Kobayashi., Applied Surface Science 216 (2003) 603–606.

[61] Kazunori Sato and Hiroshi Katayama-Yoshida., Japanese Journal of Applied Physics, 39, Pt 2, 6B (2000).

[62] Bindiya H. Soni,M. P Deshpande ,Sandip V. Bhatt, Nitya Garg, Nilesh N. Pandya, S. H Chaki., Journal of Optics, 42, 4, (2013) 328-334.

[63] J.K. Furdyna, J. Appl. Phys. **64** (1988) R29.

[64] K. Sato, H. Katayama-Yoshida, Jpn. J. Appl. Phys. 40 (2001) L334.

[65] Shubra Singh, E.Senthil Kumar, M.S. Ramachandra Rao., Scripta Materialia, 58, 10, (2008), 866–869.

[66] S.J. Pearton, W.H. Heo, M. Ivill, D.P. Norton, T. Steiner, Semicond. Sci. Technol. 19 (2004) R59.

[67] T. Dietl, Nat. Mater. 2 (2003) 646.

[68] S.G. Yang, T. Li, B.X. Gu, Y.W. Du, H.Y. Sung, S.T. Hung, C.Y. Wong, A. B. Pakhomov, Appl. Phys. Lett. 83 (2003) 3746.

[69] J.M.D. Coey, A.P. Douvalis, C.B. Fitzgerald, M. Venkatesan, Appl. Phys. Lett. 84 (2004) 1332.

[70] S.J. Pearton, C.R. Abernathy, M.E. Overberg, G.T. Thaler, D.P. Norton, N. Theodoropoulou, A.F. Hebard, Y.D. Park, F. Ren, J. Kim, L.A. Boatner, J. Appl. Phys. 93 (2003) 1.

[71] W. Prellier, A. Fouchet, B. Mercey, J. Phys.: Condens. Matter. 15 (2003) R1583.

[72] R. Janisch, P. Gopal, N.A. Spaldin, J. Phys.: Condens. Matter 17 (2005) R657.

[73] S.A. Chambers, Surf. Sci. Rep. 61 (2006) 345.

[74] S.J. Pearton, D.P. Norton, K. Ip, Y.W. Heo, T. Steiner, Prog. Mater. Sci. 50 (2005) 293.

[75] Swarup K. Neogi, Aritra Banerjee, Sudipta Bandyopadhyay., Current Physical Chemistry, (2013) 333-356.

[76] https://www.ukessays.com/essays/biology/number-of-transistor-per-square-inch-biology-essay.php (Accessed on April 4th 2016).

[77] T. Graf, S. T. B. Goennenwein and M. S. Brandt, Phys. Stat. Sol. (b) **239** (2003) 277.

[78] S. W. Jung *et al*, *Appl. Phys. Lett*. **80** (2002) 4561.

[79] Y. M. Cho, W. K. Choo, H. kim, D. Kim, Y. E.Ihm, *ibid*. **80** (2002) 3358.

[80] Nadia Febiana Djaja, Rosari Saleh., Materials Sciences and Applications, (2012) 245-252.

[81] Gunjan Srinet, Ravindra Kumar, Vivek Sajal, J Mater Sci: Mater Electron (2014) 3052–3056.

[82] O.D. Jayakumar, I.K. Gopalakrishnan, S.K. Kulshrestha, Physica B 381 (2006) 194–198.

[83] L.J. Zhuge, X.M. Wu, Z.F. Wu, X.M. Chen, Y.D. Meng, Scripta Mater. 60 (2009) 214.

[84] L. Schneider, S.V. Zaitsev, W. Jin, A. Kompch, M. Winterer, M. Acet, G. Bacher, Nanotechnology 20 (2009) 135604.

[85] B.Q. Wang, J. Iqbal, X.D. Shan, G.W. Huang, H.G. Fu, R.H. Yu, D.P. Yu, Mater. Chem.Phys. 113 (2009) 103.

[86] K. Ueda, H. Tabata, T. Kawai, Appl. Phys. Lett. 79 (2001) 988.

[87] H. Liu, X. Zhang, L. Li, Y.X. Wang, K.H. Gao, Z.Q. Li, R.K. Zheng, S.P. Ringer, B. Zhang, X.X. Zhang, Appl. Phys. Lett. 91 (2007) 072511.

[88] J.M.D. Coey, M. Venkatesan, C.B. Fitzgerald, Nat. Mater. 4 (2005) 173.

[89] K.R. Kittilstved, N.S. Norberg, D.R. Gamelin, Phys. Rev. Lett. 94 (2005) 147209.

[90] N.H. Hong, J. Sakai, N.T. Huong, N. Poirot, A. Ruyter, Phys. Rev. B 72 (2005) 045336.

[91] Y.M. Hu, C.W. Hsu, C.Y. Wang, S.S. Lee, S.J. Wang, T.C. Han, W.Y. Chou, Scr. Mater. 61 (2009) 1028.

[92] S.B. Zhang, S.-H. Wei, A. Zunger, Phys. Rev. B 63 (2001) 075205.

[93] B.K. Roberts, A.B. Pakhomov, V.S. Shutthanandan, K.M. Krishnan, J. Appl. Phys. 97 (2005) 10D310.

[94] P. Sharma, A. Gupta, K.V. Rao, F.J. Owens, R. Sharma, R. Ahuja, J.M.O. Guillen, B. Johansson, G. A. Gehring, Nat. Mater. 2 (2003) 673.

[95] H. Wang, H.B. Wang, F.J. Yang, Y. Chen, C. Zhang, C.P. Yang, Q. Li, S.P. Wong, Nanotechnology 17 (2006) 4312.

[96] Baiqi Wang, Javed Iqbal, Xudong Shan, Guowei Huang, Honggang Fu, Ronghai Yu, Dapeng Yu., Materials Chemistry and Physics, 113, (2009) 103–106.

[97] V. Pazhanivelu, A. Paul Blessington Selvadurai, Yongsheng Zhao, R. Thiyagarajan, R. Murugaraj, Physica B: Condensed Matter, 481, (2016) 91–96.

[98] Shahid M. Ramaya *et al.*, Arabian Journal of Chemistry (2013).

[99] A. El Amiri, R. Moubah, F. Lmai, M. Abid, N. Hassanain, E.K. Hlil, H. Lassri, Journal of Magnetism and Magnetic Materials, 398, (2016) 86–89.

[100] C. Zener, Phys. Rev. 81, 440-444 (1951).

[101] E. Quintero, M. Quintero, M. Morocoima, G.E. Delgado, L. Lar, J. Gomez, and P. Bocaranda, Mexican Journal Of Physics, 53 (7), (2007) 163–166.

[102] E. Quintero, R. Tovar, M Quintero, J. Gonzalez, J. M Broto, H. Rakoto, R. Barbaste, J.C Woolley, G. Lamarche, A. M Lamarche,., Journal of Magnetism and Magnetic Materials, 210, (2000) 208–214.

[103] J. Stankiewicz, F. Palacio, F. Villuendas, Acta Physica Polonica A, 92 (1997) 976-980.

[104] R. N. Gurzhi, A.N. Kalinenko, A.I. Kopeliovich, A.V. Yanousky, E.N. Bogachek, U. Landman, Phys. Rev. B 68 (2003) 125113.

[105] T. Diel, H. Ohno, F. Matsukura, J. Cibert, J. D. Ferrand, Science 287 (2000) 1019.

[106] R. Janisch, P. Gopal, N. A. Spaldin, J. Phys. Condens. Matter 17 (2005) R657e89.

[107] L.J. Zhuge, X.M. Wu, Z.F. Wu, X.M. Chen, Y.D. Meng, Scripta Mater. 60 (2009) 214.

[108] L. Schneider, S.V. Zaitsev, W. Jin, A. Kompch, M. Winterer, M. Acet, G. Bacher, Nanotechnology 20 (2009) 135604.

[109] B.Q. Wang, J. Iqbal, X.D. Shan, G.W. Huang, H.G. Fu, R.H. Yu, D.P. Yu, Mater. Chem.Phys. 113 (2009) 103.

[110] B.K. Roberts, A.B. Pakhomov, V.S. Shutthanandan, K.M. Krishnan, J. Appl. Phys. 97 (2005) 10D310.

[111] P. Sharma, A. Gupta, K.V. Rao, F.J. Owens, R. Sharma, R. Ahuja, J.M.O. Guillen, B. Johansson, G. A. Gehring, Nat. Mater. 2 (2003) 673.

[112] H. Wang, H.B. Wang, F.J. Yang, Y. Chen, C. Zhang, C.P. Yang, Q. Li, S.P. Wong, Nanotechnology 17 (2006) 4312.

[113] J. Das, S.K. Pradhan, D.R. Sahu , D.K. Mishra, S.N. Sarangi, B.B. Nayak, S. Verma, B.K. Roul, Physica B 405 (2010) 2492–2497.

[114] Mei Li, Gu Li, Juan Jiang, Zishou Zhang, Xin Dai, Kancheng Mai, Journal of Materials Science & Technology (2015) 331–339.

[115] S.Abdullahi, M.Momoh,H.N.Yahya, IOSR Journal Of Environmental Science, Toxicology And Food Technology (2013) 81-85.

CHAPTER THREE

EXPERIMENTAL DETAILS

3.1 Sample Preparation

From the view point of research as well as commercial use, it is very much desirable and important to adopt appropriate synthesis techniques to prepare single phase pure materials free from any type of contamination. Material synthesis is the most important part of research, it can determine the properties of the material. In the current work, we have prepared the samples by using solid state reaction described below.

3.1.1 Solid State Reaction

Solid state reaction route (SSRR) has been adopted to prepare polycrystalline samples of (Cr) doped ZnO bulk ceramics. Appropriate proportion of high pure oxides of Zn and Cr (Puraterm-99.999%) were used for the synthesis of $Zn_{1-x}Cr_xO$ (x= 0.01, 0.05 and 0.09) pellets. Weighed amount of powders of the oxide were ground properly for about 2 hours using an agate mortar. The powders were heated at 400 ^{0}C for six hours then followed by room temperature quenching and grinding. The procedure was repeated five times in order to achieve homogeneous mixture of green powder with smaller particle size. The powders were pelletized after mixing with Poly Vinyl Alcohol (PVA) as binder. Cylindrical pellets with approximately 2 mm thickness and 10 mm diameter were prepared using a hydraulic press with 30 ton base capacity and pressure of 10 ton / cm^2 showed in figure 3.1. The pelletized material were sintered at 500 ^{0}C and 800 ^{0}C for 8h using a vacuum furnace fitted with a programmable (Eurotherm controller, Model: 2404) temperature controller [1].

Figure 3.1: Hydraulic press used in this work.

3.1.2 Slow Step Sintering Schedule

Proper sintering process is adopted to increase the inter particle contact area, achieve maximum physical densification, control grain growth, minimize the volume of inter-connected pores in the samples as well as to control shrinkage without geometrical deformation. For the current work, we adopted a novel slow step sintering schedule, which could help to have a systematic and refined grain growth as well as ensure reproducibility of the synthesized material with definite composition and properties with a control on the defect / vacancy states in the system effectively [1].

3.2 Sample Characterization

In the current work $Zn_{1-x}Cr_xO$ produced by solid state reaction have been characterized using scanning electron microscopy (SEM), X-Ray diffraction (XRD) spectrometer, Fourier

Transform InfraRed spectrometry (FTIR), Ultraviolet–visible spectroscopy (UV-Vis), Raman spectroscopy, Photoluminescence Spectroscopy (PL), Superconducting quantum interference devices (SQUID) and Electron Spin Resonance technique (ESR). To investigate the microstructure and topography the SEM was used. The XRD has been used to investigate the crystal structure. In order to investigate the optical properties and defect structure of $Zn_{1-x}Cr_xO$ the PL has been used. We have employed the UV-Vis to investigate the optical band gap and the FTIR to investigate the bonding and molecular composition present in our sample. The Electron Spin Resonance (ESR) technique was used to probe the electromagnetic response of the samples $Zn_{1-x}Cr_xO$ (x= 0.01, 0.05, 0.09). We have also used Raman analysis to investigate incorporation of dopant and defects in the structure. The techniques and working principles of equipment used are discussed in the following section.

3.2.1 Scanning Electron Microscopy (SEM)

SEM is a very suitable characterization tool for the microstructural studies of any sample. It provides better resolution than that of optical microscope. The SEM has two main components which are the electron column and the electronic console [2-3]. There are adjustable knobs and switches in the electron console which are responsible for contrast and brightness, magnification, regulating and adjusting accelerating voltage and filament current. The main purpose of the electron column is to focus, generate and scan the electron beam on the sample [2-3]. The beam produced at the top of the microscope by the electron gun is focused downward on the sample which travels through the lenses and the electromagnetic field. SEM functions by focusing the electrons beam at a point to scan the surface of the sample. When the beam hits the sample several interactions takes place [4], various forms of signals are realized such as the backscattered electrons, Auger electrons, secondary electrons,

X-ray, and cathadoluminescence. The SEM image generation is usually by the backscattered electrons and secondary electrons.

The electron beam hitting the sample surface produces the secondary electrons and the backscattered electrons. The secondary electrons have energies less than 50 eV and they are as a result of the inelastic collision and the scattering of incident electrons on the surface of the sample. The structural surface of the material is confirmed by secondary electrons by resolution of ~10nm or more while the backscattered electrons are a result of elastic interactions of the incident electrons and the sample nuclei [5, 2]. The electron beam which comes from the electron gun is used to create a SEM image when the sample surface is scanned (See Figure 3.2).

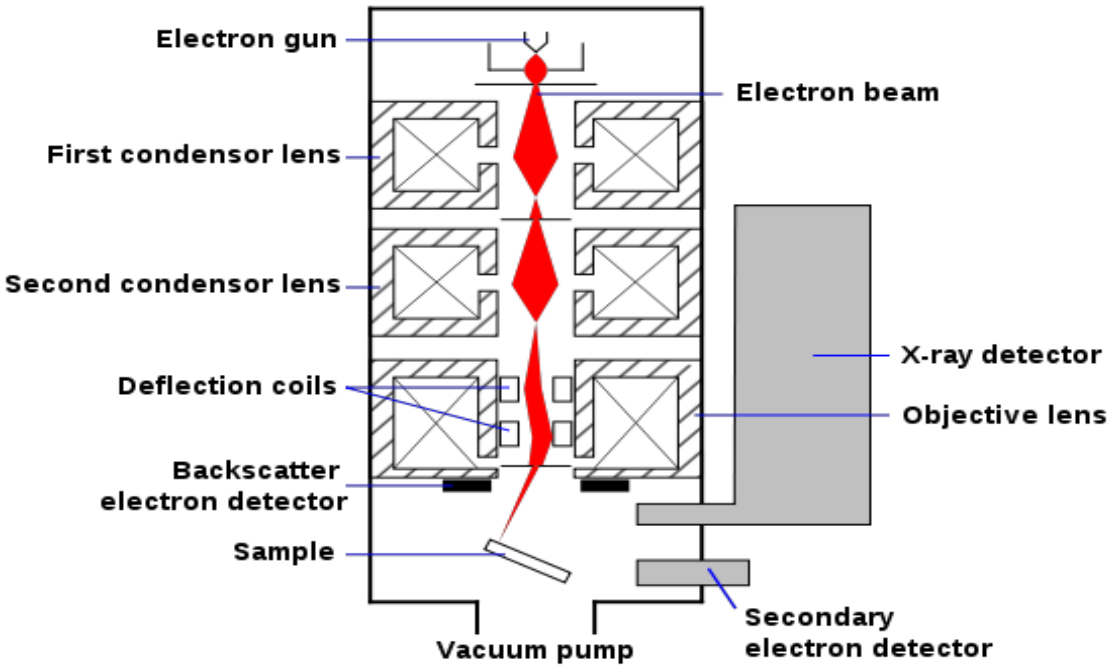

Figure 3.2: Schematic block diagram of SEM [8].

Several points on the specimen surface will emit electrons that are sensed by the electron detector [6,7].

3.2.2 X-Ray diffraction spectrometer (XRD)

The X-ray diffraction (XRD) is a very useful tool in determining the crystal structure of a sample under study. XRD data can be used to determine the grain size and lattice constant [9-11]. The operation of XRD stems from Bragg's law. It involves the directed X-Ray beam being pointed on the sample. Diffraction occurs when the rays hits the sample [12]. The different crystalline structures present in the samples $Zn_{1-x}Cr_xO$ were determined using the XRD.

In crystal, atoms are arranged in such a way that small volume can be identified due to their regular pattern in three dimensions which makes the whole crystal [13]. When X-rays are incident on them and are seen to scatter in all directions. But when the atoms inside a material are periodically arranged, then the scattered X-rays are seen to be diffracted and interfere with each other as seen in Figure 3.3. It is seen that at this angle 'θ', Bragg's law is satisfied and the scattered X-rays intensity is higher in regards to the incident angle scanned [14]. The data from XRD is plotted as intensity against the diffracted x-rays and the peaks which are seen is said to satisfy Bragg's law. Equations 3.1 and 3.2 show Bragg's and Scherrer's equations respectively. From Scherrer's equation the crystallite size can be computed from XRD data [14].

$$2d \sin\theta = n\lambda, \tag{3.1}$$

where θ is scattering angle, n is positive integer, λ is the wavelength of X-ray.

$$\tau = \frac{K\lambda}{\beta \cos\theta} \tag{3.2}$$

where τ is the crystallite size, K is the shape factor, λ is wave length, β is full width at half maximum (FWHM) in radians obtained from different values of (2θ), θ being the Bragg's angle.

In this thesis, XRD patterns of $Zn_{1-x}Cr_xO$ samples were recorded with Philips diffractometer (Model 1715) using Cu Kα tube with wavelength λ = 1.540593 Å.

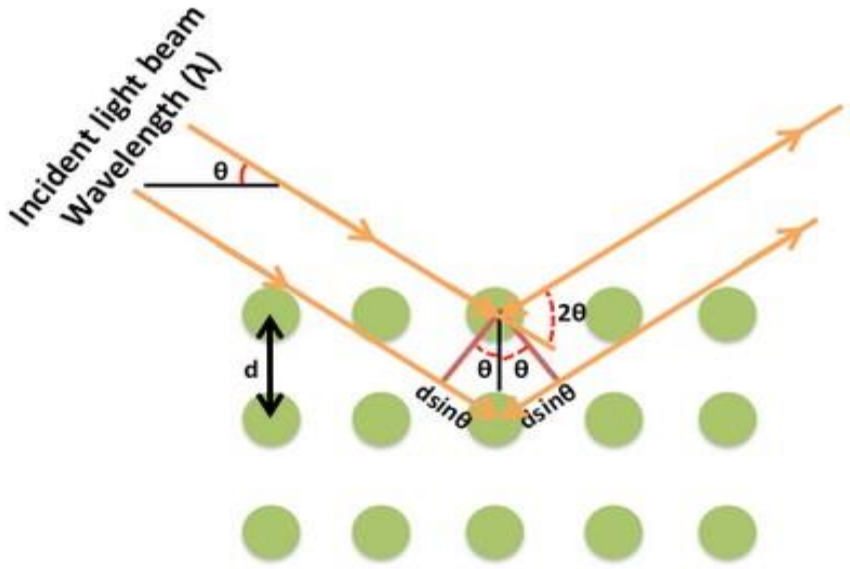

Figure 3.3 XRD in crystals [16].

3.2.3 Fourier Transform InfraRed spectrometry (FTIR)

To study the elemental composition and chemical bonding of any sample, the Fourier Transform InfraRed spectrometry (FTIR) is an effective tool to use. The sample is exposed to InfraRed radiation from the (FTIR) set up, the sample absorbs some of the infrared radiation and some of the infrared is transmitted.The FTIR can analyze samples up to the scale of microns to kilometers, which can give information about bonding and chemical composition

in the elements. The interferometer in FTIR spectrometer generates the interferogram, the faster sampling and good signal is as a result of the wavelengths been measured simultaneously in the FTIR instrument [17,18]. The Michelson interferometer is commonly used in FTIR and is made up of two perpendicular plane mirrors, one of the plane mirrors travels in perpendicular direction of the plane which is a semi-reflecting film that cut across the plane of the mirrors. Light is passed from a light source to the beam splitter, half of that light is reflected to one of the mirrors and the other half is transmitted to the other mirror. These mirrors reflect these two beams returning them to the beamsplitter where they combine and interfere [19]. Figure 3.4 shows the layout of a simple FTIR spectrometer.

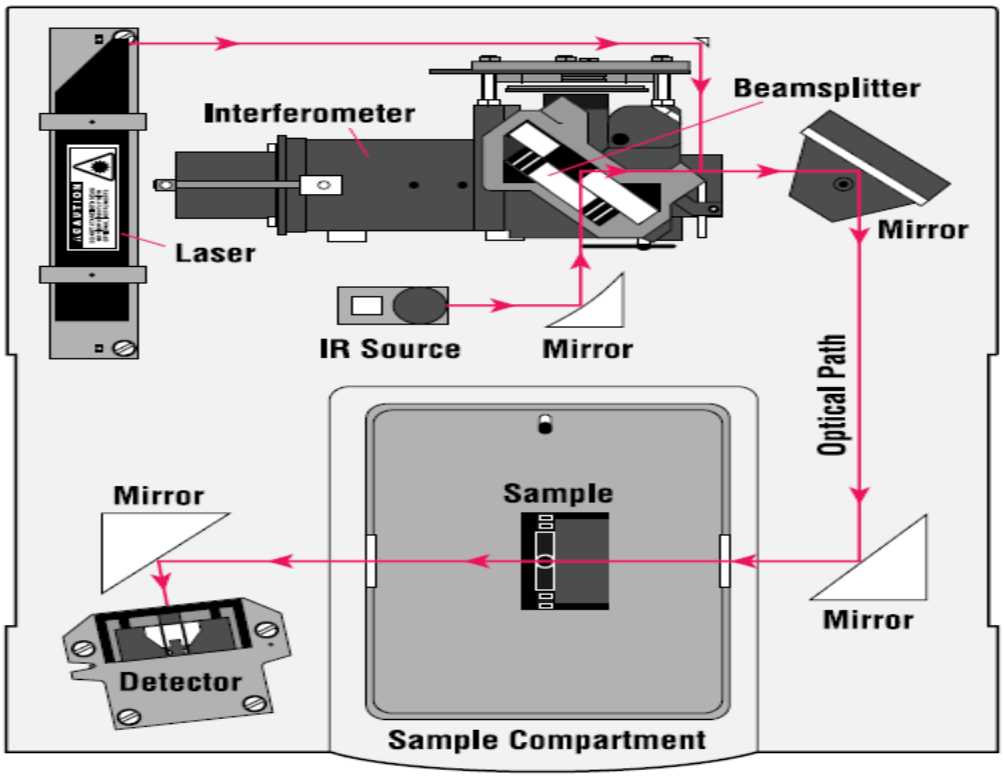

Figure 3.4: Layout of FTIR spectrometer [20].

The samples $Zn_{1-x}Cr_xO$ (x= 0.01, 0.05, 0.09) were mounted in the FTIR sample holder and pressed down by a rotating arm which presses the sample to the crystal pot to get good contact before the spectrum is obtained.

3.2.4 Ultraviolet–visible spectroscopy (UV-Vis)

Ultraviolet–visible spectroscopy (UV-Vis) is an absorption spectroscopy that allows a molecule to absorb light in ultra-violet region of 200-400 nm and visible region of 400-800 nm which results in excitation of electrons to higher energy state from ground state [21] in the region of 1.5- 6.2 eV associated with electromagnetic spectrum. The absorbance spectra of a sample in a solid form or a compound in solution is obtained using a UV-Vis spectrometer. It uses a light source from a tungstem lamp or deuterium, also included in it is a sample holder and detector. One wavelength can be selected at a time for a UV-Vis that has a filter or monochromator in it. Some UV-Vis spectrometer has a diode array detector instead of a monchromator for detecting absorbance simultaneously at all wavelengths [22]. Figure 3.4 shows electron excited from ground state to higher energy. Wavelength is absorbed when the amount of energy is enough to make electronic transitions [21].

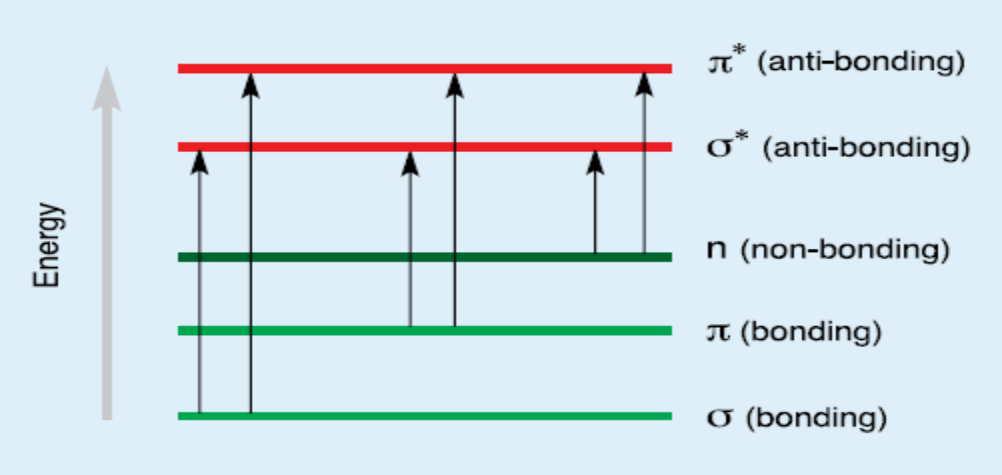

Figure 3.5: Electronic transitions [21].

Some of the different types of UV-Vis spectrometer are single beam spectrometer, double beam spectrometer and simultaneous spectrometer.

The wavelength of the incident radiation builds upon the various kinds of spectroscopy shown on in figure 3.6 below. The UV-Vis spectroscopy provides details of the transition of external electrons of atoms absorbed by UV-Vis radiation at different wavelength which is used for the identifications of elemental composition from the emitted spectrum or the spectrum absorbed.

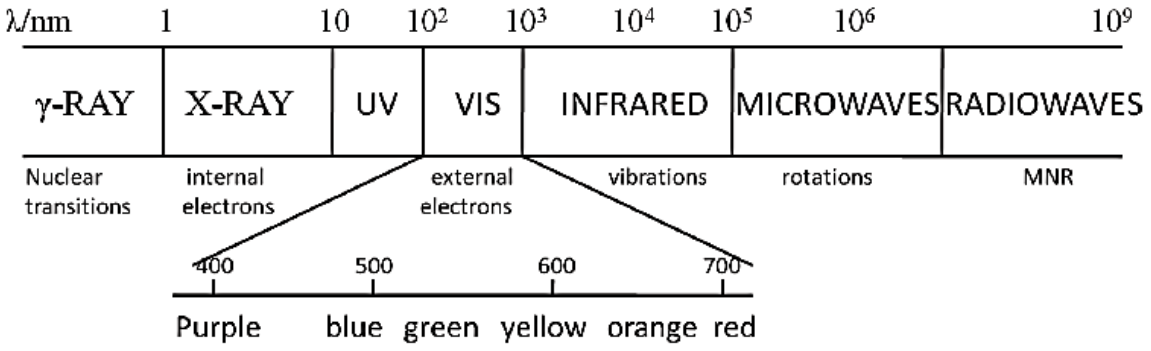

Figure 3.6: Electromagnetic spectrum with wavelength radiation [23].

3.2.4.1 Transmittance and Absorbance

The amount of light absorbed as light goes through a material or reflected from the material gives the difference in the transmitted radiation denoted by I and incident radiation is denoted by I_o. Transmittance and absorbance is expressed in terms of amount of light absorbed by the material. Transmittance and absorbance can be defined as follows,

For transmittance, it is given in terms of fraction of 1 or in percentage,

$$T = I/I_O \text{ or } \%T = (I/I_O) \times 100 \qquad (3.3)$$

And for absorbance,

$$A = -\log T \qquad (3.4)$$ [22].

We have used the PerkinElmer Lambda 1050 UV-Vis spectrometer (figure 3.8) to estimate the optical bandgap in the sintered samples of $Zn_{1-x}Cr_xO$ (x= 0.01, 0.05, 0.09).

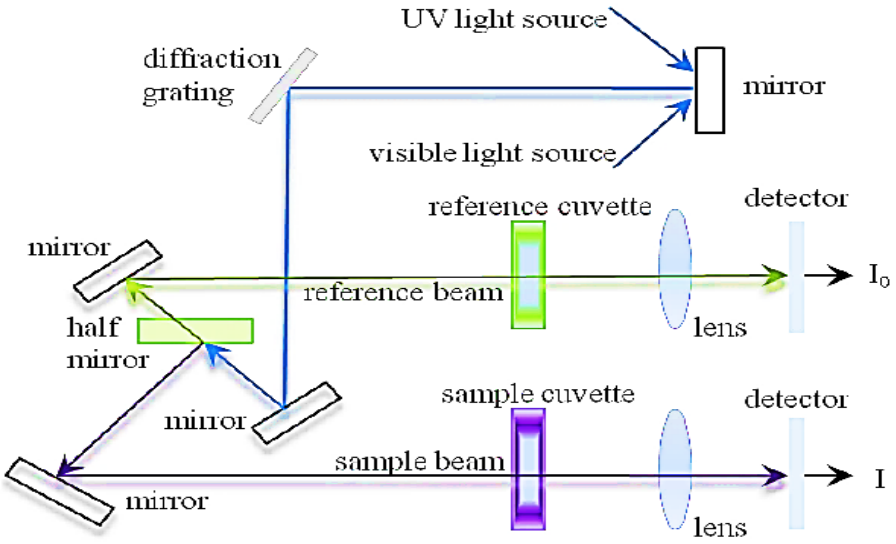

Figure 3.7: Diagram of UV-vis spectroscopy [25].

Figure 3.8: A Picture of PerkinElmer Lambda 1050 UV-vis spectroscopy.

3.2.5 Raman spectroscopy

Raman spectroscopy involves the scattering of electromagnetic radiation as a result of atoms and molecules. This spectroscopy examines low frequency nodes [26]. Vibrations in molecules can be detected using spectroscopies based on Raman scattering processes and infrared absorption. This can be used to get information about the chemical structures of a sample. Physical forms can also be detected. Particle size as well as size distribution is measured using simple scattering technique even to a size of less than 1 µm. In Raman spectroscopy, a single radiation frequency is used in order to irradiate the sample resulting in radiation scattered from the sample. The incident beam is different from the vibrational unit of energy. The energy difference of the excited and ground states does not need to match the incident radiation. The electrons around the nuclei is distorted when the light combines with the molecule. It is a short-lived state known as the virtual state. It is not a stable state because the photon is radiated again instantly [27]. This process is known as Rayleigh scattering. Optical and vibrational oscillations interact when the molecule's electron cloud is distorted from the molecular vibrations which results to a process known as Raman scattering [28]. Figure 3.9 shows the Raman scattering and Rayleigh scattering process.

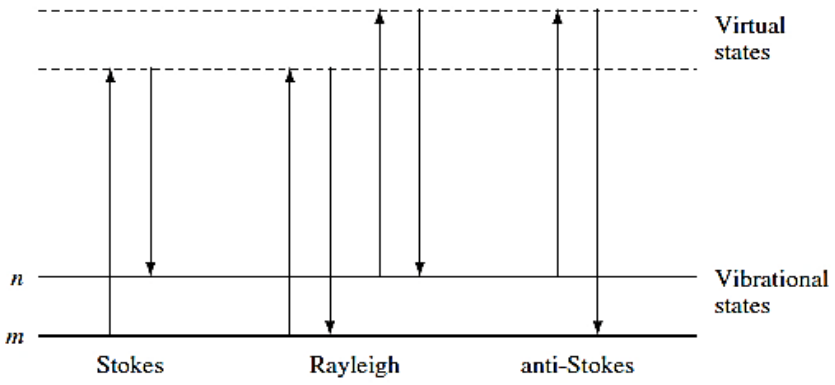

Figure 3.9: Raman scattering and Rayleigh scattering process [27].

The absorption energy of the molecule is as the result of the ground vibrational state *m* from the Raman scattering process and the advancement to higher energy vibrational state *n* known as Stokes scattering.

A plot of Raman intensity versus Raman shift gives the Raman spectrum. The Raman shift in the spectrum are the Raman band parameters, the band and its intensity are directly related to the molecular structure [29]. The range of Raman spectra can be from 4000-10 cm^{-1}, but vibrations of organic molecules in Raman active normal modes are at 4000-400 cm^{-1} [29, 30]. Figure 3.10 shows the block diagram of Raman spectrometer.

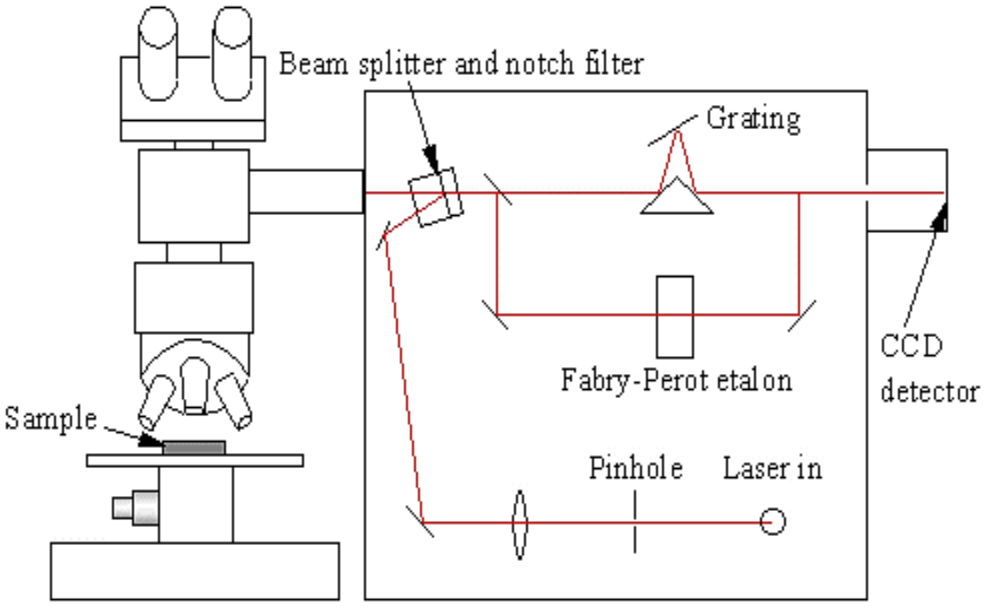

Figure 3.10: Block diagram of a Raman spectrometer [31].

In this work, the Jobin Yvon T64000 Raman spectrometer equipped with an Ar ion laser (515 nm) has been used. The laser power on the sample was 5 mW, and the spectra were recorded over a 20s period having LASER beam spot size of ~1 µm.

Figure 3.11: A picture of Jobin Yvon T64000 Raman spectrometer

3.2.6 Photoluminescence (PL) Spectroscopy

Photoluminescence involves the absorption of energy, also with emission of light. This is usually referred to as luminescence. PL is a nondestructive technique used to investigate optoelectronic, intrinsic and extrinsic properties and also the electronic structure of a sample. Photoluminescence (PL) can be used to understand and determine the purity level, band gap and defects present in the material [32,33]. When the sample absorbs light and enough energy is imparted into the material, it results to a process known as photo-excitation. The only way the sample can dissipate this surplus energy is by the emission of light. The electrons inside material in its permissible excited state is due to the photo-excitation. The surplus energy is released when the electrons get back to their state of equilibrium and may or may not carry emission of light [33].

Photoluminescence consist of phosphorescence and fluorescence. It is from the process of absorption and emission as result of various energy levels in the sample. The PL

depends on the type of sample under study and the laser wavelength. In order to avoid unwanted phosphorescence, the appropriate laser wavelength must be used [34].

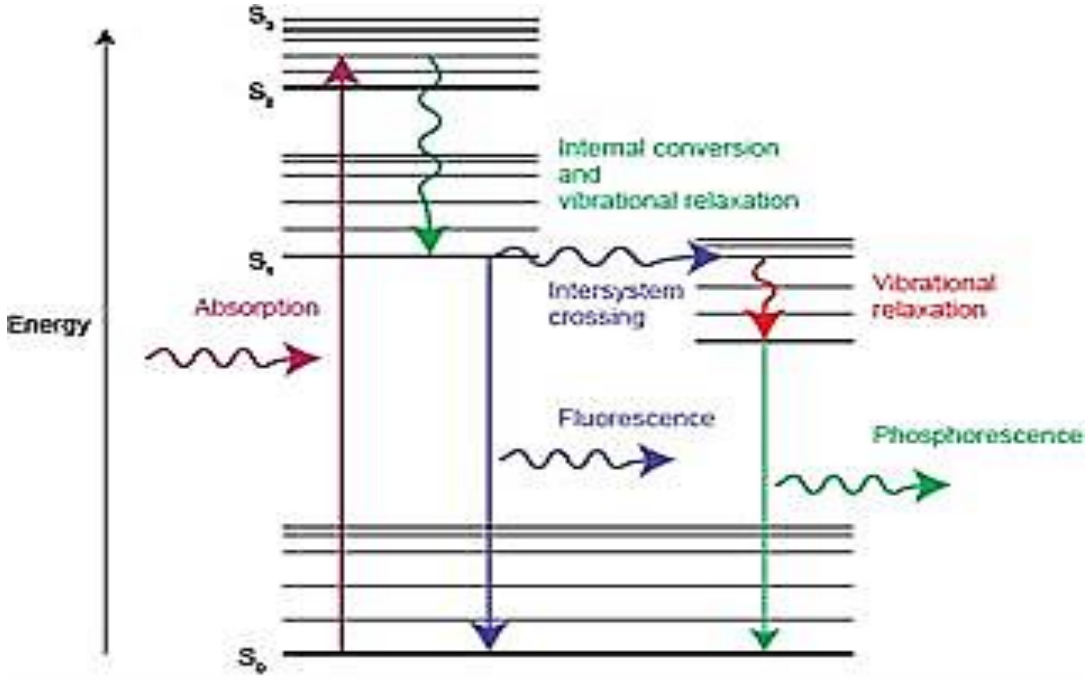

Figure 3.12: Energy level of absorption of light and emission of light [36].

The PL spectral can be obtained as a result of measuring the excitation wavelength and the intensity of the emitted radiation from the material under study. By monitoring the emission on a fixed wavelength as well as vary the excitation wavelength the excitation spectrum is obtained. The intensity of the emitted radiation and a fixed wavelength from the excited material is used to obtain the emission spectrum [35].

In this work, Photoluminescence (PL) study on $Zn_{1-x}Cr_xO$ (x= 0.01, 0.05, 0.09) samples was performed using Fluorolog-3 spectro-flourometer attached with a 450 W xenon lamp, using 325 nm excitation.

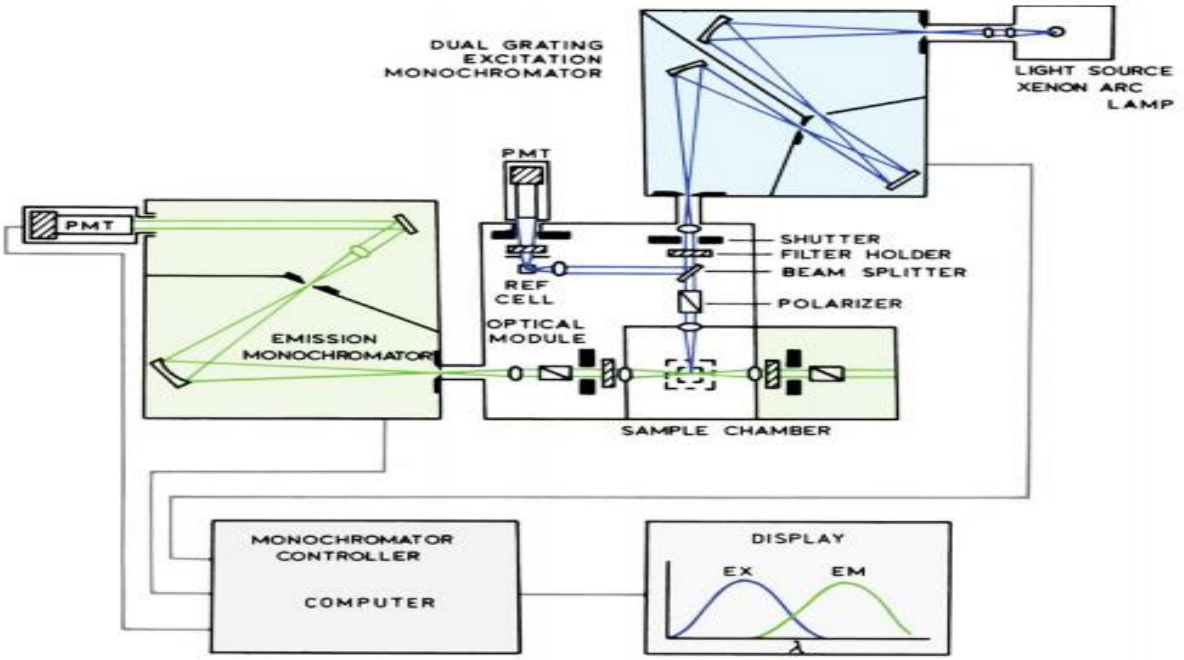

Figure 3.13: Schematic diagram of a Photoluminescence (PL) [36].

Figure 3.14: Image of Photoluminescence (PL) used in this work

3.2.7 Electron Spins Resonance Spectroscopy

The electron spin resonance spectroscopy is also referred to as electron paramagnetic resonance (EPR). It was invented in 1945 by Zavoisky, a Russian physicist [41]. It involves

electromagnetic radiation absorption which is similar to other spectroscopy. As a spectroscopy, it measures and interpret the energy difference between the atomic or molecular states due to systems with unpaired electrons with spin state S = 1/2 [42].

In ESR, the energy difference measured is a result of the unpaired electrons and the applied magnetic field from electromagnetism in the ESR. The energy difference ΔE is obtained from the equation 3.5 which is the resonance condition.

$$\Delta E = h\nu, \qquad (3.5)$$

where ν is the frequency of the radiation and h is the planck constant [43].

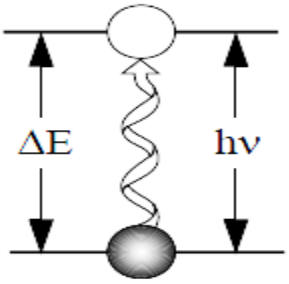

Figure 3.15: Absorption of electromagnetic energy [44].

The change of energy from the lower state to higher energy state is due to the absorption of energy as shown in figure 3.15. In ESR, the energy difference is due to Zeeman effect [44]. The difference between the energies of the higher energy state and lower energy state is as result of interaction between the magnetic field and the electron spin as shown in (equation 3.6).

$$\Delta E = g\,\mu_B\,B_0\,\Delta m_s \qquad (3.6)$$

where g is the g-factor and it is a proportionality constant approximately equal to 2 for most samples, μ_B is Bohr magneton, m_s is total spin angular moment, s is spin quantum number, Δm_s is change in spin state usually equal to ±1 [44,45].

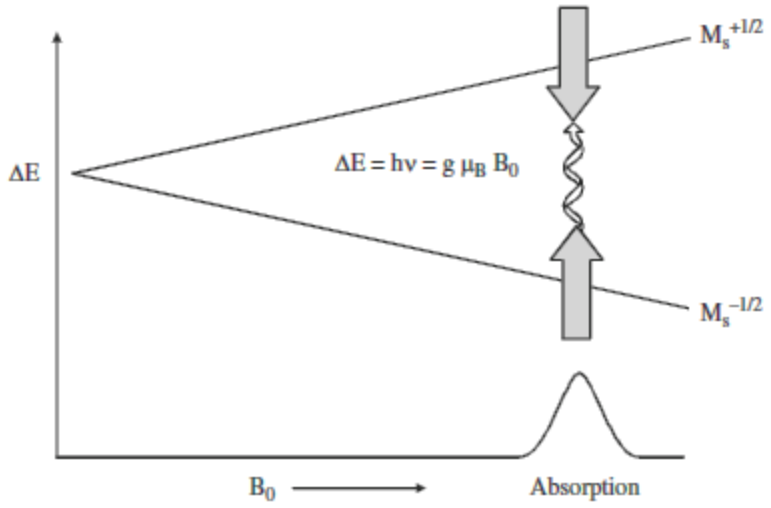

Figure 3.16: Resonance condition of ESR [45].

For the two spin states transition to occur, there must be energy differences which is given by equation 3.7,

$$\Delta E = h\nu = g\,\mu_B B_0 \quad \text{and} \quad \mu_B = g_e\,\beta/2 \qquad (3.7)$$

where g_e is the g-factor, μ_B is Bohr magneton and B_0 is the applied magnetic field.

If there is no applied magnetic field the two spin states will have the same energy which results in no energy difference to measure. From figure 3.16, there is linear divergence in the energies of the two spin state when the magnetic field is increased. In order to obtain a spectrum the electromagnetic radiation frequency is kept constant while the magnetic field is varied. If the energy of the radiation matches the energy difference of the two spin states, an absorption peak is formed due to the magnetic field applied to the two spins. This field is known as the resonance field [42].

In the ESR, the klystron generates the microwave, which is the source [41]. The radiant energy frequency is around 9.5 GHz for microwave region. The Klystron is a low-

noise vacuum tube. The attenuator is used to adjust the microwave power that the sample sees inside the cavity. The sample cavity which is also known as the resonator amplifies the small signal from the sample in the sample cavity and the microwave enters the resonator by an iris [46]. The detector, usually a diode is used to reflect the microwave resonated from the sample cavity [44].

Electron spin resonance (ESR) study is a well-established powerful technique, which can effectively investigate the microscopic details of spin dynamics of electrons inside the system leading to the diverse magnetic behaviours. It is highly sensitive to detect para- and ferromagnetic phases, anisotropy, magnetic inhomogeneity, high frequency loss, defect centers and spin splitting g factor in novel multifunctional materials. It is reported that it is capable of detecting 10^{11} spins at room temperature [37 - 39].

When exposed to microwaves, magnetic materials exhibit resonance phenomena in the presence of an external magnetic field satisfying Larmor's condition. The line width of the absorption peaks, resonance field, g factor and integral intensity can provide information about the magnetic ordering inside the system. The fine structure of ESR spectra indicates the effective spin and local environment. Its amplitude predicts magnetization, hyperfine structure reflects coupling to nuclear spins and spin relaxation provides information about dynamic coupling with neighbouring spins [41]. ESR on polycrystalline samples gives facts on the description of ferromagnetism due to the extrinsic inter-growth defects and the intrinsic short range order. All components of the ESR are shown in figure 3.17.

Bruker EMX spectrometer (figure 3.18) operating at 9.45 GHz is equipped with an oxford ESR 910 continuous flow cryostat and a field modulation frequency of 100Hz is used in this work to investigate the magnetic response of $Zn_{1-x}Cr_xO$ (x= 0.01, 0.05 and 0.09) diluted magnetic semiconductor. Interesting results were obtained which will be discussed in chapter four of this report.

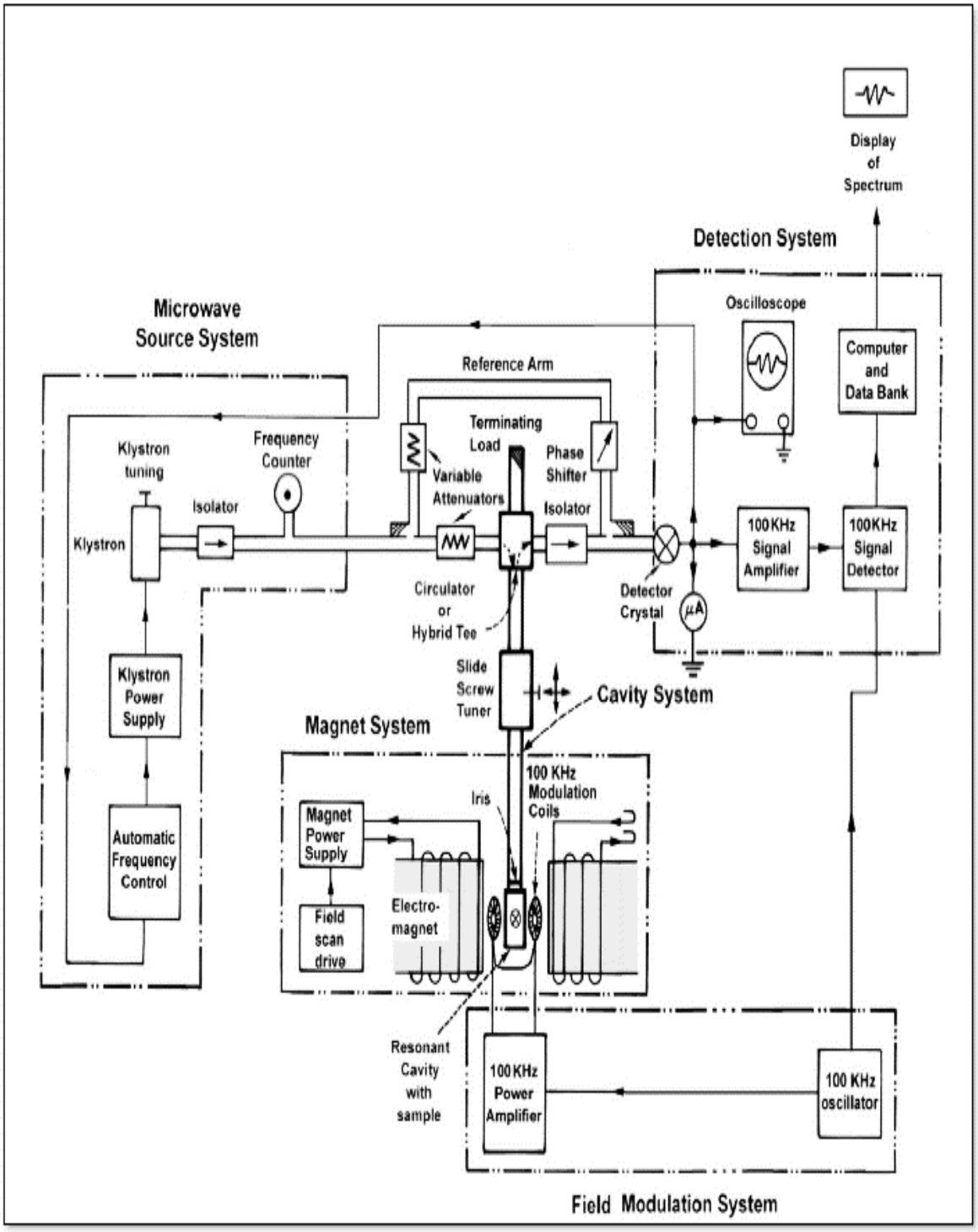

Figure 3.17: Block diagram of Electron Spin Resonance Spectrometer [48].

Figure 3.18: ESR Bruker EMX spectrometer used in this work

3.2.8 Superconducting quantum interference devices (SQUID)

The SQUID uses the phenomena of Josephson tunneling and flux quantization, it is very sensitive to magnetic flux [47, 49], it measures the output voltage signal and magnetic flux. The output voltage and magnetic flux is as result of the periodic function of a flux [48, 50, 51]. SQUID is able to detect small magnetic fields and can measure fields to the range of 10^{-15} T. It has a central element that is made up of a ring of semiconducting material [52].

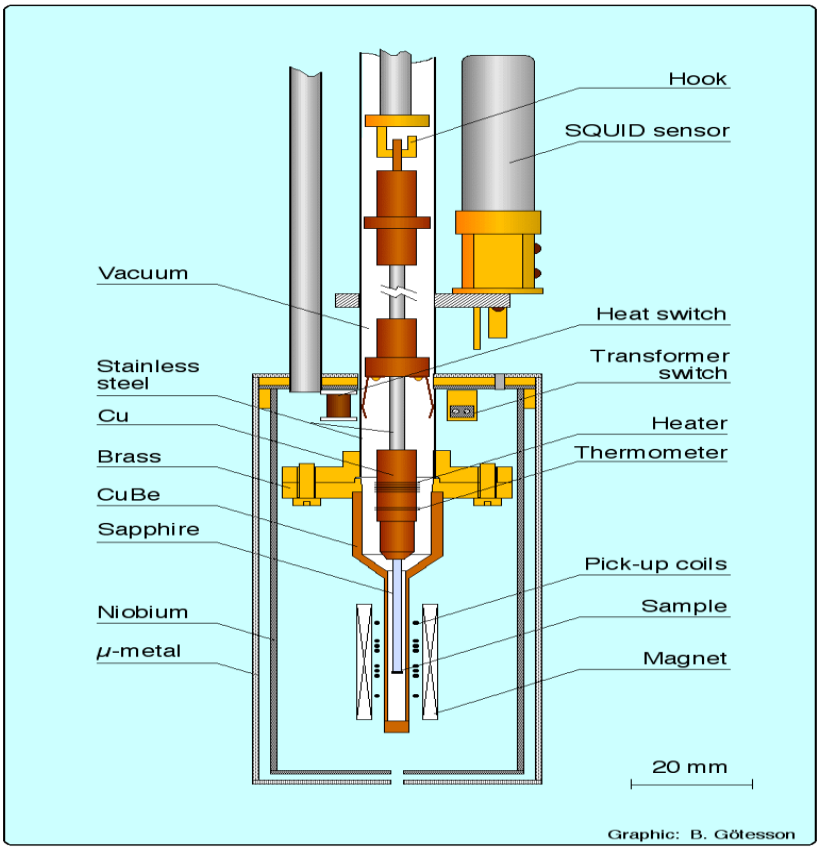

Figure 3.19: Schematic diagram of SQUID Magnetometer [54].

The SQUID functions essentially as a superconducting sensor [48]. We have used the SQUID set up in this thesis to detect the magnetization of the samples $Zn_{1-x}Cr_xO$ (x= 0.01, 0.05, 0.09). The samples were mounted on the sample holder and then placed in the gap of the magnet. The gap magnet supplies the static magnetic field. Magnetic measurements of the samples were recorded at room temperatures (300K) and low temperature (10K) using SQUID with maximum field of 10,000e.

The SQUID magnetometer was used for the following:

3.2.8.1 Magnetization and Applied field (Hysteresis)

Here a magnetic field was applied and swept from zero up to a positive value such that saturation magnetization was reached and then back through zero to a negative value and then

back to the positive value through zero field. The parameters obtained from hysteresis measurement were coercivity (Hc), saturation magnetization (Ms) and saturating field (Hs).

3.2.8.2 Zero-field-cooled (ZFC) magnetization

The sample was cooled in zero field A small magnetic field, necessary to probe the system was applied at the lowest temperature, and the magnetization recorded on heating.

3.2.8.3 Field-cooled (FC) magnetization

The sample was cooled in a small field down to the lowest temperature, while the magnetization was recorded. One could also collect the magnetization on re-heating.

3.3 References

[1] J. Das, S.K. Pradhan, D.R. Sahu , D.K. Mishra, S.N. Sarangi, B.B. Nayak, S. Verma, B.K. Roul, Physica B 405 (2010) 2492–2497.

[2] http://www.sjsu.edu/people/anastasia.micheals/courses/MatE143/s1/SEM_GUIDE.pdf (accessed on 1st February 2016).

[3] Ramanjeet Kaur, International Journal of IT, Engineering and Applied Sciences Research, (2015) 1-7.

[4] Bindell, J. Scanning Electron Microscopy. Encyclopedia of Materials Characterization: Surfaces, Interfaces, Thin Films, ed. Brundle, R. and C. Evans. (1992) pp70-83.

[5] Hafner B ,Scanning Electron Microscopy Primer, Characterization Facility.University of Minnesota, Twin Cities, USA, (2007) pp1-29.

[6] Larry D. Hanke, P E, Hanbook of Analytical Methods for Materials, Material evaluation and Engeneering, USA. (2001) pp35-38.

[7] Onyancha R. B, Non-Resonant Microwave Absorption Studies in SmFeAs(O,F) Iron Pnictide Superconductor, University of South Africa, South Africa, (2015) (Msc Thesis).

[8] http://piyushcharan.yolasite.com/resources/NANO_NOTES/Scanning%20Electron.pdf (Accessed 2nd February).

[9] Zachariasen, W.H. and E.L. Hill, The Theory of X-ray Diffraction in Crystals. The

Journal of Physical Chemistry, 1946. **50**(3): p. 289-290.

[10] Ryland, A.L., X-ray diffraction. Journal of Chemical Education, 1958. **35**(2): p. 80.

[11] Dorset, D.L., X-ray Diffraction: A Practical Approach. Microscopy and Microanalysis, 1998. **4**(05): p. 513-515.

[12] S. H. Tolbert, A. P. Alivisatos, Annu. Ev. Phys. Chem., **1995**, 46, 595

[13] C. Suryanarayana, M. Grant Norton. X-Ray diffraction: a practical approach, Plenum Press, New York, (1998) p. 63-94.

[14] Cullity, B.D., Elements of x-ray diffraction. Addison-Wesley Pub. Co. (1978) p. 1-25.

[15] Tony S. Price, Nonlinear Properties of Nanoscale Barium Strontium Titanate Microwave Varactors, University of South Florida, 2012, (PhD Thesis).

[16] http://archive.cnx.org/contents/517f8f37-f619-4408-a8b4-2ef8a53e8c29@2/wide-angle-x-ray-diffraction-studies-of-liquid-crystals

(accessed on 1st February 2016).

[17] Bogolitsyn, K.G., Physical-chemical analysis methods. 2001, Archangelsk: ASTU publishing.

[18] Otto M. Modern methods of analytical chemistry. Moscow, Technosphere, (2003) p. 281.

[19] B. Stauart., Infrared Spectroscopy: Fundamentals and Applications. John Wiley & Sons, Ltd, (2004) p. 1-70.

[20] http://mmrc.caltech.edu/FTIR/FTIRintro.pdf (accessed on 12th March 2016).

[21] http://www.rsc.org/learn-chemistry/resource/download/res00000282/cmp00001304/pdf (accessed on 17th March 2016)

[22] Brittany L. Oliva-Chatelain and Andrew R. Barron., Basics of UV-Visible Spectroscopy, OpenStax-CNX module: m34525, (2010) 1-6.

[23] http://lafactoria.lec.csic.es/mcc/attachments/article/40/100385-CharctXSol.pdf (accessed on 1st February 2016).

[24] Tony Owen., Fundamentals of modern UV-visible spectroscopy, Agilent Technologies, (2000) p. 1-58.

[25] https://www.researchgate.net/figure/277312936_fig1_Figure-1-Schematic-diagram-of-a-UV-vis-spectroscope (accessed on 1st April 2016).

[26] Travis Thompson., Fundamentals of Raman Spectroscopy, Laser Focus World, (2012) p. 2-16.

[27] Smith E, Dent G. Modern Raman spectroscopy – a practical approach., Chichester: John Wiley & Sons Ltd. (2005) p. 1-61.

[28] McCreery RL. Raman spectroscopy for chemical analysis., NewYork: John Wiley & Sons, Inc. (2000) p. 1-12.

[29] Gauglitz G, Vo-Dinh T. Handbook of spectroscopy., Weinheim: Wiley-Vch Verglag GmbH & Co. KGaA. (2003) p. 557-558

[30] BUMBRAH, G. S., SHARMA, R. M., Egyptian Journal of Forensic Sciences, (2015) 1-6.

[31] http://www.chm.bris.ac.uk/pt/diamond/stuthesis/chapter2.htm (accessed on 14th April 2016).

[32] G. D. Gilliland, Mater. Sci. Eng. R18, (1997) 99.

[33] Ruquan Ye and Andrew R. Barron., Photoluminescence Spectroscopy and its Applications., OpenStax-CNX module: m38357, (2001) p. 1-11.

[34] http://www.renishaw.com/en/photoluminescence-explained--25809 (accessed on 14th April 2016).

[35] http://chemwiki.ucdavis.edu/Core/Analytical_Chemistry/Analytical_Chemistry_2.0/10_Spectroscopic_Methods/10F%3A_Photoluminescence_Spectroscopy (accessed on 14th April 2016).

[36] J. R. Lakowicz., Principles of Fluorenscence Spectroscopy., Springer, (2006) p. 206-210.

[37] D. Toloman, A. Mesaros, A. Popa ,O. Raita, T.D. Silipas, B.S. Vasile, O. Pana, L.M. Giurgiu, Journal of Alloys and Compounds 551 (2013) 502–507.

[38] L.S. Vlasenko and G.D.Watkins, Phys. Rev.B 72 (2005) 035203.

[39] J.Lee, J Kim, and K. H. Kim, Phys. Status. Solidi A 211, (2014) 1900.

[40] B.M.Weckhuysen et al, Mol. Sieves (2004) 4: 295–335.

[41] Philip .H. Rieger, Electron Spin Resonance: Analysis and Interpretation., The Royal Society of Chemistry. (2007) p. 1-11.

[42] http://www.auburn.edu/~duinedu/epr/1_theory.pdf (accessed on 14th April 2016).

[43] Anders L, Shiotani M and Shimada S, Principles and Applications of ESR Spectroscopy Springer, Dordrecht Heidelberg London New York., (2011) p. 3-28.

[44] R. T. Weber, J. J. Jiang, D. P. Barr, EMX User's Manual. EPR Division, Bruker Instruments, Inc., 19 Fortune Drive, Manning Park, Billerica, MA 01821, (1998) p. 1-24.

[45] Gareth R. Eaton., Sandra S. Eaton., David P. Barr., Ralph T. Weber., Quantitative EPR, SpringerWienNewYork., (2010) p. 1-14.

[46] Weil J and Bolton J, Electron Paramagnetic Resonance, 2nd ed., J. Wiley, USA. (2007) p. 7-50.

[47] The SQUID handbook vol II: Fundamentals and technology of SQUIDs and SQUID systems" J. Clarke and A. I. Braginski eds. Wiley-VCH Verlag GmbH & Co. KgaA, Weinheim, (2006) p. 29-86.

[48] Nagendran Ramasamy and Madhukar Janawadkar., SQUID Based Nondestructive Evaluation, Indira Gandhi Centre for Atomic Research, Kalpakkam, India, (2012) p. 26-52.

[49] John Clarke, Michael Hatridge, and Michael Mößle., Annual Review of Biomedical Engineering, 9, (2007) 389-413.

[50] J G Park., Journal of Physics F: Metal Physics, 3, Number 6, (1973) 1144.

[51] G. Aviv, SQUIDs- Superconducting Quantum Interference Devices, Department of Physics, Ben-Gurion University of the Negev, Experimental physics course (2008) 1-9.

[52] Asma Khalid, Rabiya Salman and Sabieh Anwar., Principles and Applications of Superconducting Quantum Interference Devices (SQUIDs), LUMS School of Science and Engineering, (2010) 1-5.

[53] http://hyperphysics.phy-astr.gsu.edu/hbase/solids/imgsol/squide.gif

[54] http://supercondutividade.blogspot.co.za/2013/08/aplicacoes-dos-supercondutores.html

CHAPTER FOUR

STRUCTURAL, OPTICAL, AND MAGNETIC PROPERTIES OF Cr DOPED ZnO

4.1 Structural Properties

4.1.1 SEM Analysis

Scanning electron microscopy studies for morphological analyses were carried out using SEM (Philips FEG Xl'30). The scanning electron micrographs of Cr doped ZnO samples are presented in Figure 4.1. The micrographs of 500 °C and 800 °C sintered $Zn_{0.99}Cr_{0.01}O$ samples are observed to show the arrangement of micro-grains uniformly throughout the surface.

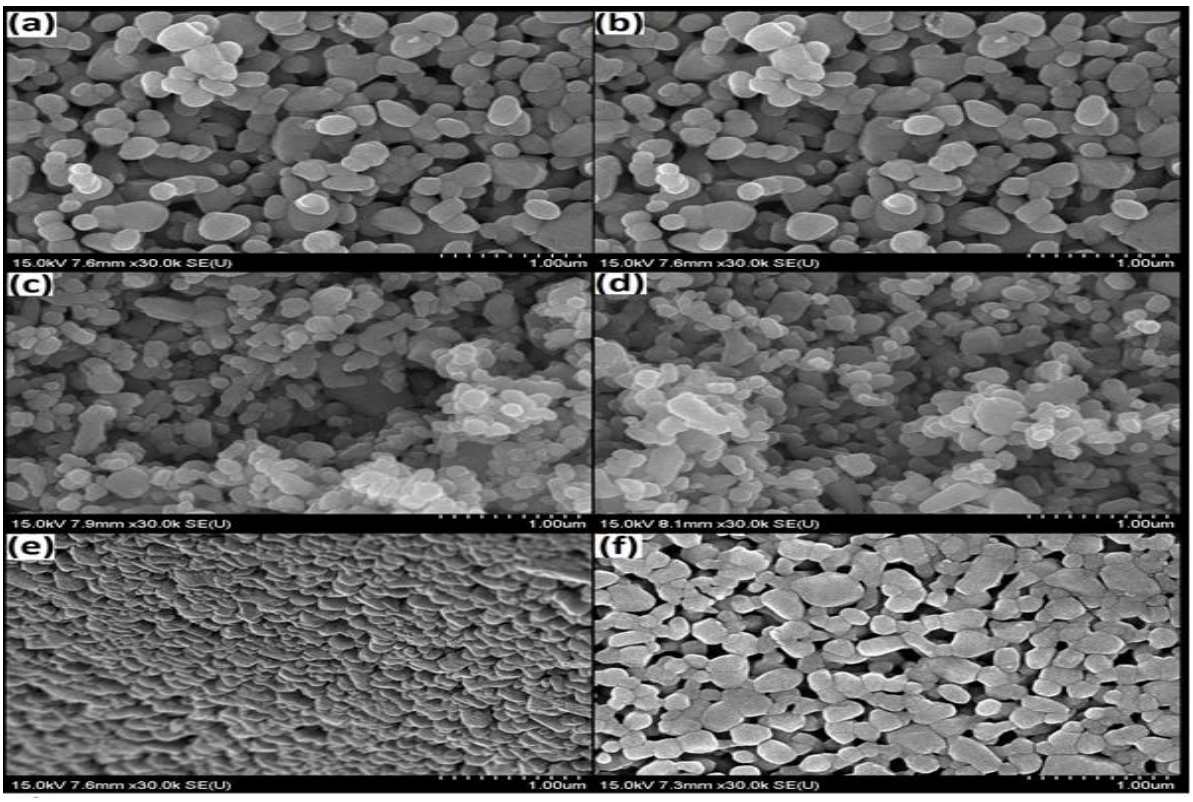

Figure 4.1: Scanning electron micrographs of polycrystalline $Zn_{1-x}Cr_xO$ ($0.01 \leq x \leq 0.09$).

Whereas an inhomogeneity in the shape and size of $Zn_{0.95}Cr_{0.05}O$ and $Zn_{0.91}Cr_{0.09}O$ samples sintered at 500 °C is observed, the same is seen to be somehow reduced in the 800 °C sintered samples. In the 500 °C sintered $Zn_{0.91}Cr_{0.09}O$ samples the arrangement of grains is closer to each other with low volumetric pore percentage, which might be the cause of higher magnetism observed for this sample which is discussed later. The micrograph of this sample shows the arrangement of both large and small grains. The average grain size in this case is more in comparison to other samples.

4.1.2 XRD Analysis

To analyse the crystalline nature of the samples and verify the incorporation of Cr into the ZnO structure, XRD study has been performed on the doped samples. In the XRD patterns presented in Figure 4.12 all the ZnO peaks are indexed to $P6_3$ mc space group with lattice parameters a = 3. 252 Å and c = 5.206 Å. Lattice Geometry equation (equation 4.1 and 4.2) was used to calculate the lattice parameters such as the lattice constant *a* and *c*, interplanar spacing *d*, and unit cell volume [1].

$$\frac{1}{d^2} = \frac{4}{3}\left(\frac{h^2 + hk + k^2}{a^2}\right) + \frac{l^2}{c^2} \tag{4.1}$$

$$V = \frac{\sqrt{3}a^2c}{2} \tag{4.2}$$

where *hkl* is the Miller indices.

A small impurity peak is detected for the sample of $Zn_{0.99}Cr_{0.01}O$ sintered at 500 °C temperatures which is identified as a chromium oxide peak. This disappeared after annealing at 800 °C. When the dopant concentration is 5%, impurity peaks corresponding to Cr_2O_3 appear and are also present in the samples doped at 9% sintered at 500 °C and 800 °C.

However, additional peaks corresponding to CrO_2 phase are detected only in the samples doped at 9%, sintered at 500 °C and 800 °C. The decreasing FWHM value with the increasing sintering temperature (Figure 4.12 inset) suggests increased crystalline nature with the sintering temperature. Peak shifts of all the doped samples sintered at 500 °C and 800 °C presented in Fig. 4.13 and Fig 4.14 respectively show slight shift of the (101) peak towards higher 2θ value with increased dopant concentration of Cr. This is due to incorporation of Cr^{3+} ions with radii 0.064 nm into Zn (0.074 nm) sites. Calculation from Williamson-Hall analysis listed in Table 4.1 and 4.2 indicates an increase in the strain value with increasing dopant concentration for the 500 °C sintered samples.

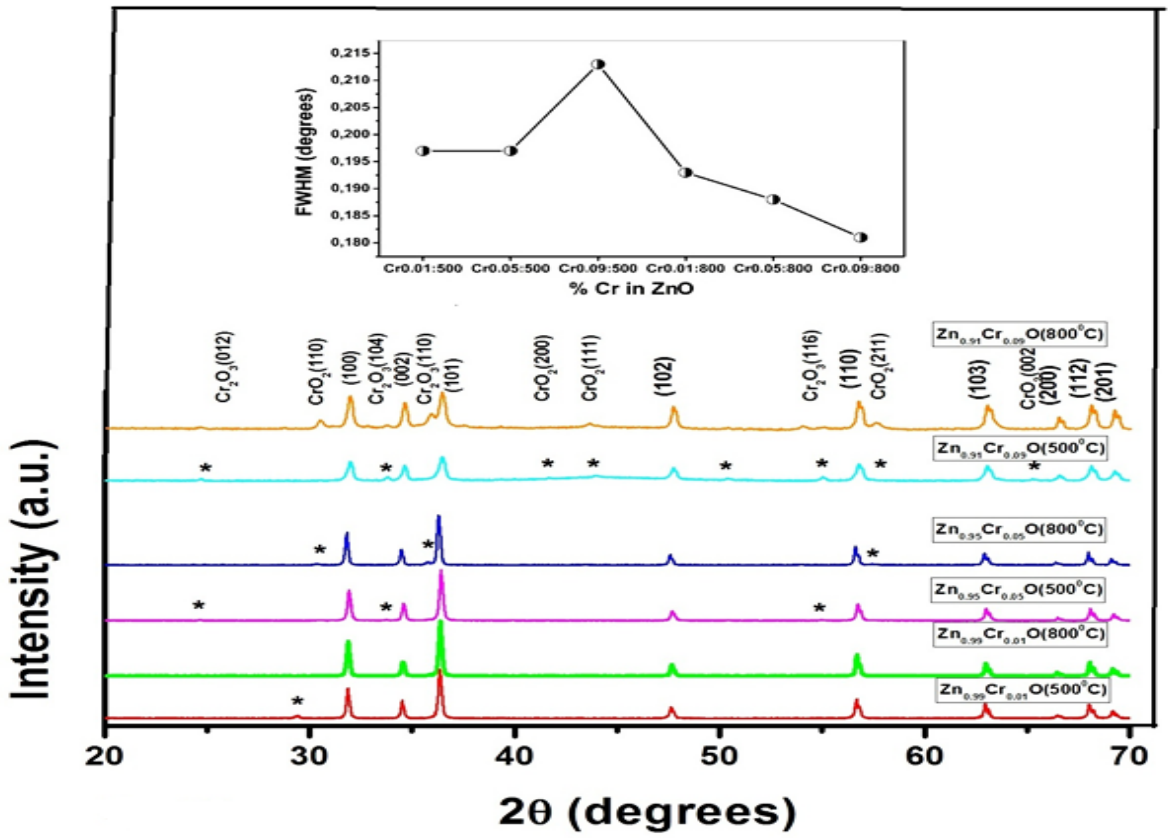

Figure 4.12 X-ray diffraction patterns of $Zn_{1-x}Cr_xO$ ($0.01 \leq x \leq 0.09$). Inset: Variation of FWHM with Cr concentration in $Zn_{1-x}Cr_xO$ at sintering temperature of 500 °C and 800 °C.

This gives rise to a decrease in the crystallite size. For 800 °C sintered samples an improved crystallite growth has been observed; the change in the size with dopant concentration has been very small. There is almost no change in the c/a value, bond length, interplaner spacing and small change in the cell volume of the samples (Table 4.1 and Table 4.2), which suggest negligible lattice distortion of ZnO due to Cr doping. The stress introduced by Cr impurity phases and corresponding strain give rise to a change in the unit cell volume. However, the appearance of CrO_2 phase in the 9% doped samples and observed ferromagnetic behaviour for the sample indicates a partial Cr ions substitution in the host lattice site of this sample.

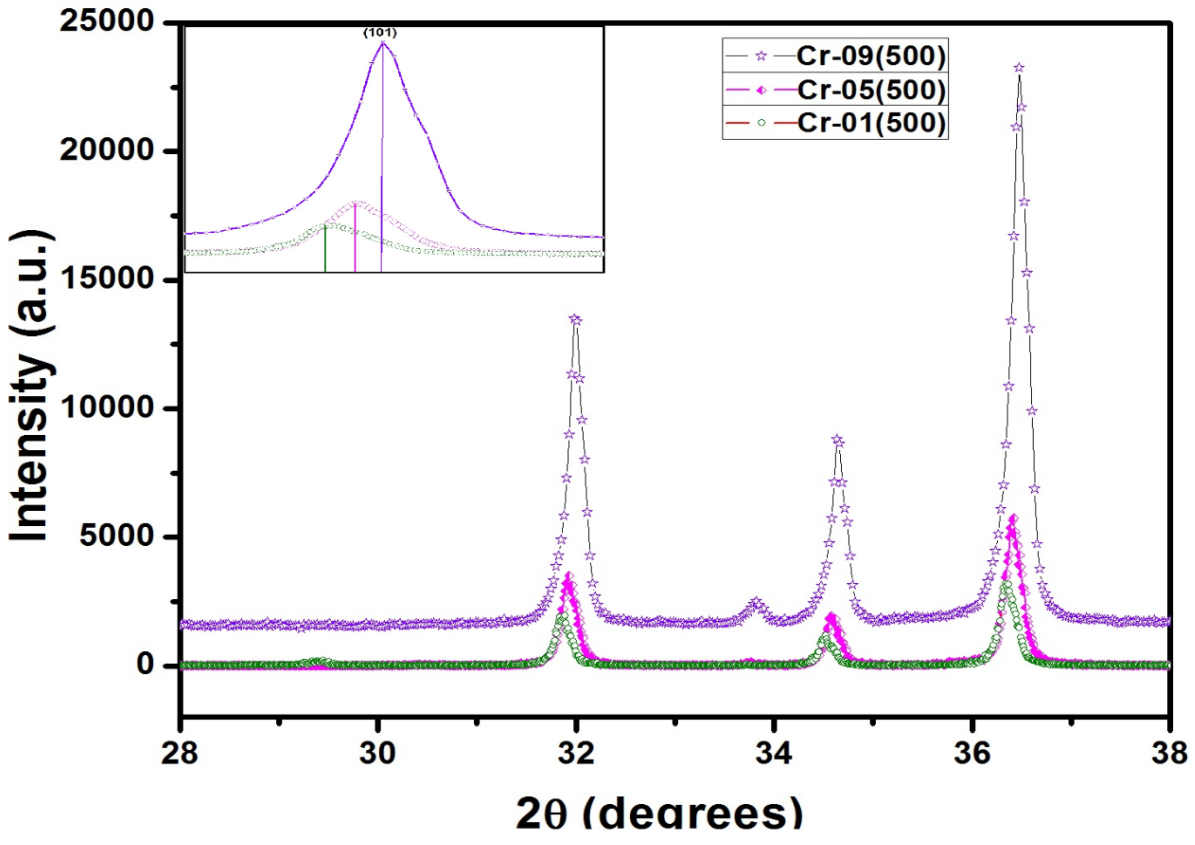

Figure 4.13: XRD (101) peak shift of $Zn_{1-x}Cr_xO$ ($0.01 \leq x \leq 0.09$) sintered at 500 °C

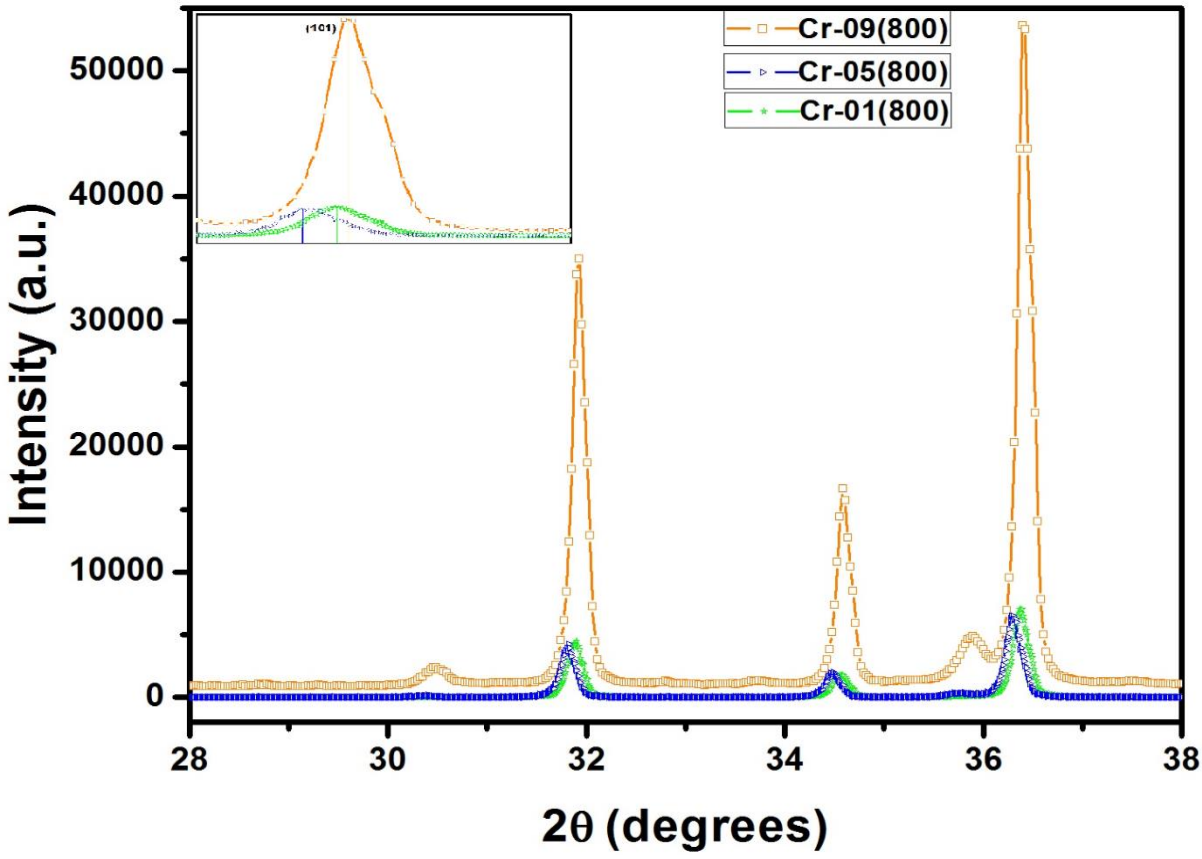

Figure 4.14: XRD (101) peak shift of $Zn_{1-x}Cr_xO$ ($0.01 \leq x \leq 0.09$) sintered at 800 °C

Table 4.1: Lattice parameter, unit cell volume in $Zn_{1-x}Cr_xO$ samples sintered at 500 °C and 800 °C.

Samples	Lattice Parameters				Unit cell Volume		c/a	
	Sintered at 500 °C		Sintered at 800 °C		Sintered at 500 °C	Sintered at 800 °C	Sintered at 500 °C	Sintered at 800 °C
	'a' in Å	'c' in Å	'a' in Å	'c' in Å				
$Zn_{0.99}Cr_{0.01}O$	3.255	5.176	3.256	5.175	47.50	47.54	1.590	1.589
$Zn_{0.95}Cr_{0.05}O$	3.255	5.178	3.252	5.172	47.54	47.38	1.590	1.590
$Zn_{0.91}Cr_{0.09}O$	3.257	5.177	3.256	5.173	47.57	47.52	1.589	1.588

Table 4.2: Strain, crystallite size, optical band gap in $Zn_{1-x}Cr_xO$ samples sintered at 500 °C and 800 °C.

Samples	Strain (10^{-3})		Crystallite size in nm (Scherer formula)		Optical band gap in eV (Tauc plot)	
	Sintered at 500 °C	Sintered at 800 °C	Sintered at 500 °C	Sintered at 800 °C	Sintered at 500 °C	Sintered at 800 °C
$Zn_{0.99}Cr_{0.01}O$	.719	1.0	36.68	37.59	3.163	3.142
$Zn_{0.95}Cr_{0.05}O$	.790	1.1	34.07	38.04	3.157	3.138
$Zn_{0.91}Cr_{0.09}O$	1.2	1.0	31.93	38.15	3.149	3.1.9

4.1.3 FTIR Analysis

For element composition study FTIR spectra was obtained from IRTracer-100 (Shimadzu).

To study the element composition of the samples sintered at 500 °C and 800 °C, FTIR spectroscopy was performed and the spectra are presented in Figure 4.15 (a) and (b) respectively. The main absorption band corresponding to Zn-O stretching mode is observed around 430 cm^{-1} for 1% doped sample sintered at 500 °C with a shoulder at 540 cm^{-1} which is shifted gradually towards lower wavenumber when the dopant concentration increases. But in the 800 °C sintered samples all the three peaks are located at the same wavenumber.

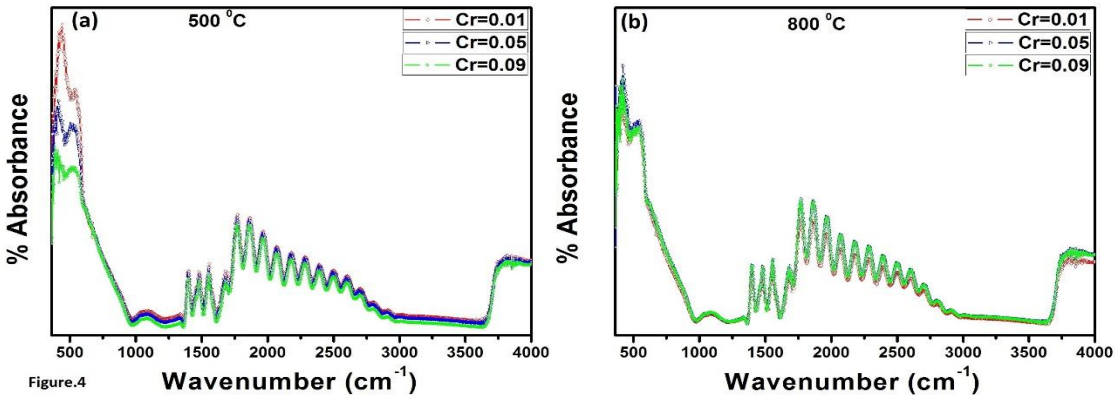

Figure 4.15: FTIR Spectra of $Zn_{1-x}Cr_xO$ (a) sintered at 500 °C and (b) sintered at 800 °C

Peaks observed around 1330 cm^{-1} correspond to H-O-H bending vibration due to the moisture in the samples. The broad absorption peak around 3800 cm^{-1} represents the stretching vibration of O-H group and absorption peaks around 2300-2400 cm^{-1} are due to C-O bonds [2, 3]. However, Cr doping and sintering in ZnO has introduced additional peaks as well peak shifts of different vibrational modes.

4.1.4 UV-Vis Analysis

Optical absorbance spectra of the samples were recorded in the range 360-800 nm as shown in Figure 4.16. It is observed that the absorption band edge shifts towards higher wavelength with increasing Cr contents in the samples. Optical band gaps in the Cr doped ZnO samples are calculated from the Tauc relation: $\alpha h\upsilon = A (h\upsilon - E_g)^{2}$; extrapolation of Tauc plot (inset Figure 4.16) shows decrease in the band gap with increasing Cr concentration in ZnO.

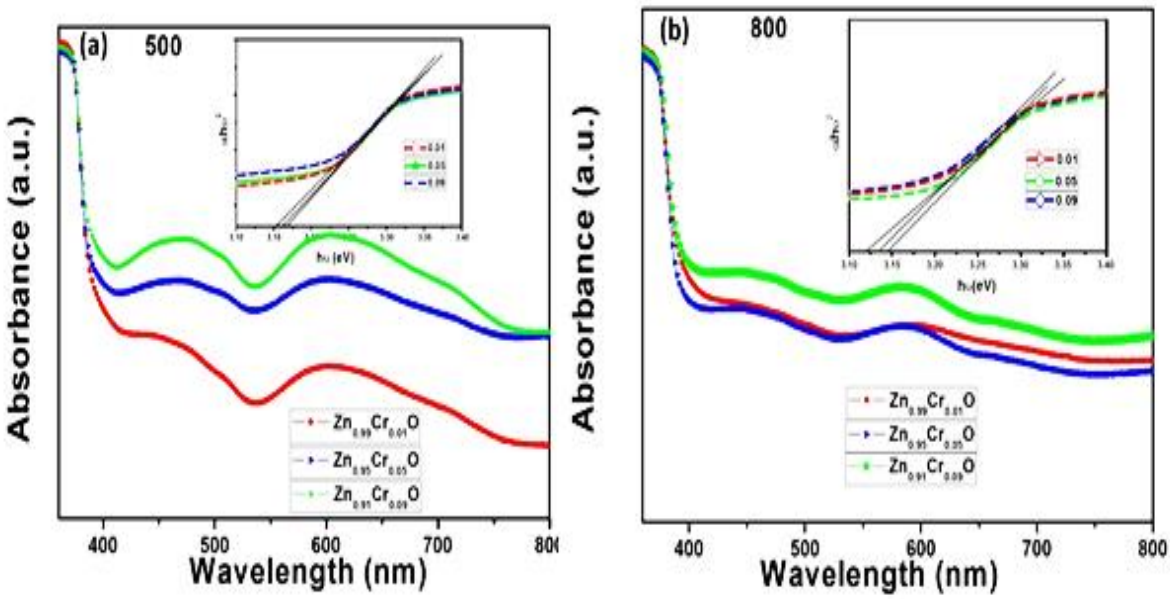

Figure 4.16 UV-Vis Spectra of $Zn_{1-x}Cr_xO$ (a) sintered at 500 °C and (b) sintered at 800 °C

This narrowing of band gap is due to Cr doping which introduces allowed energy states in the band gap of ZnO. It is presumed that there has been the sp-d exchange interaction between band electrons of ZnO and localised d electrons of Cr dopants [4].

4.1.5 Photoluminescence (PL) Analysis

For optical spintronics devices, it is necessary to create transparent magnetic semiconductors that can show optical emission at room temperature. To explore more into optical property and its relation with defects, photoluminescence (PL) is performed on all the doped samples. Figure 4.17 and Figure 4.18 presents the PL spectra of the Cr doped ZnO samples sintered at 500 °C and 800 °C respectively. The spectra for samples sintered at 500 °C (Figure 4.17) consisted of two parts: narrow peak in the ultraviolet (UV) region and another in visible light (Vis) region. In UV region, the emission peak is at 378 nm which is generally originated from the near-band-edge (NBE) excitonic transition in wide band gap of ZnO [5, 6]. The observed slight blue-shift of the emission peak (from 382 to 378 nm) might be due to spin-correlated exciton formation and crystal deformation through Cr doping and indicates that Cr doping can slightly tune the energy level and band gap of ZnO, which is also confirmed in the UV-Vis study.

In visible region, two peaks are observed at 441 nm and 533 nm for all the doped samples. The strong blue emission band centred at 441 nm for all the samples sintered at 500 °C is attributed to the transitions between the shallow donor levels of Zn interstitial to the top of the valence band [7] or the transitions between shallow acceptor levels of oxygen vacancies and shallow donor levels of zinc vacancy [8]. The mechanism of the green luminescence at around 500-550 nm in ZnO is correlated to oxygen vacancies [9], in which the emission results from the recombination of photo generated hole with an electron occupying the oxygen vacancy [10, 11]. The deep level emission band at 553nm is quite suppressed, which indicates

that the existence of Cr dopants can enhance the excitonic recombination radiation [12]. The narrow width and low intensity of the green emission peak at 553nm points towards the presence of oxygen vacancies in the three samples. Up to now, researchers have demonstrated that the defects or oxygen vacancies have significant influence on the magnetic property of materials [13, 14]. In the spectra of 800 °C of Figure 4.18, the UV emission band located at 378 nm is broader in width as compared to the 500 °C sintered samples. As for the Cr-doped ZnO, more electrons caused by chromium dopants take up the energy levels located at the bottom of conduction band. When they are excited by the laser of 325 nm, the excitons take up higher energy levels at the bottom of the conduction band.

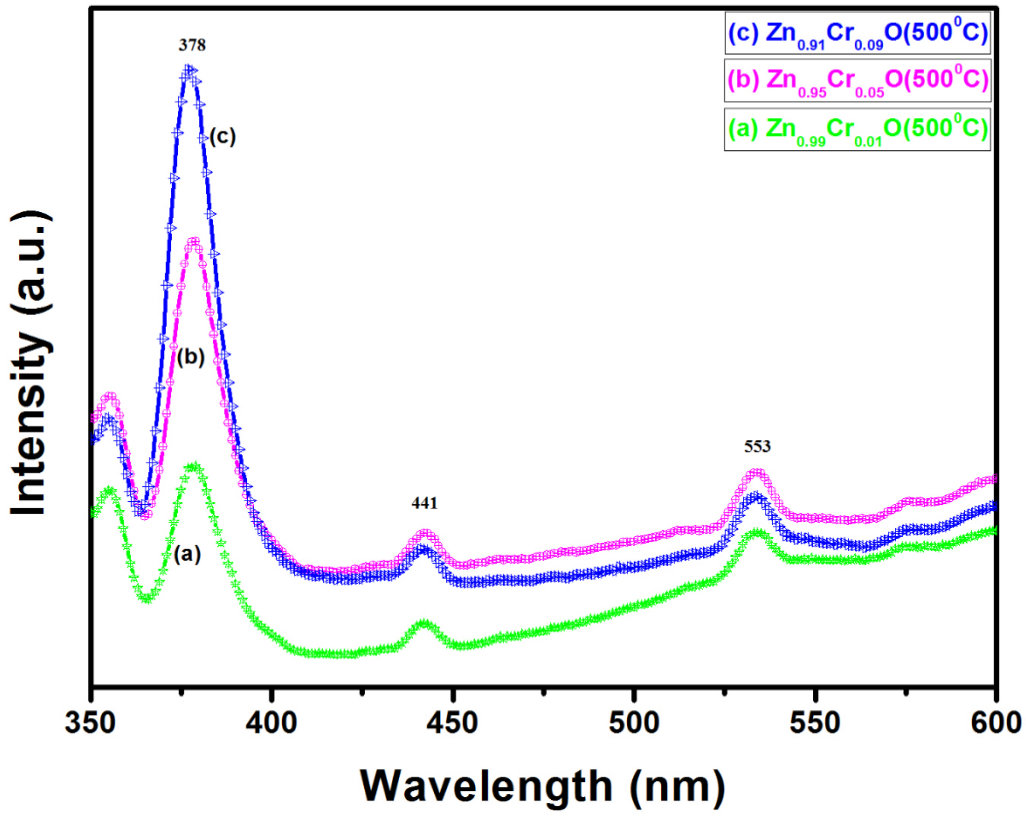

Figure 4.17 Photoluminescence spectra of $Zn_{1-x}Cr_xO$ ($0.01 \leq x \leq 0.09$) sintered at 500 °C

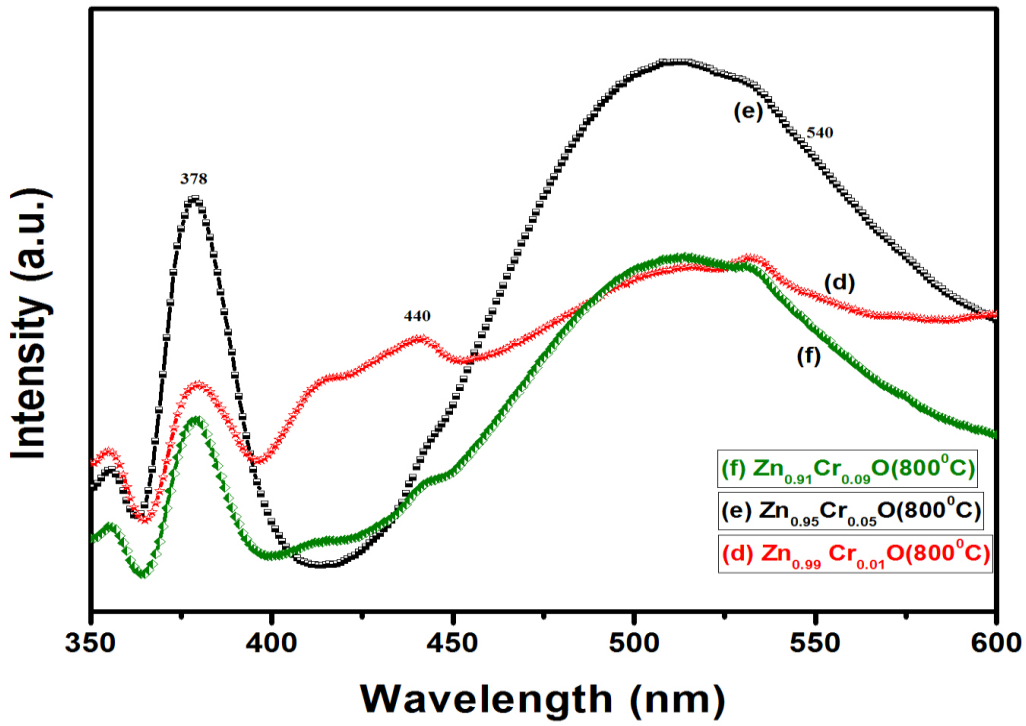

Figure 4.18 Photoluminescence spectra of $Zn_{1-x}Cr_xO$ ($0.01 \leq x \leq 0.09$) sintered at 800 °C.

The radioactive recombination of these excitons may lead to blueshift and the broadening of the UV emission peak [15]. In the deep level visible emission region, each of the three Cr doped samples sintered at 800 °C, display a broad defect-related visible luminescence band in the range of 440–540 nm. The broad visible green emission observed demonstrate that the samples have considerable defects mostly in the form of oxygen vacancy and clusters. However, it is significant to notice that both the UV emission peak and the deep level emission peak have been reduced in intensity for the 9 at. % doped samples, as compared to 1% and 5% Cr doped samples, which may be an indication that Cr-Cr interaction has been assisted by oxygen vacancies to yield fair magnetisation value in these samples as discussed later.

When the ratio of UV peak intensity to visible I_{UV}/I_{vis} was calculated, it was observed that the ratio of 5% and 9% Cr doped ZnO sintered at 500 °C and the 9% Cr doped sample

sintered at 800 °C is higher as compared to that of 1% doped sample, indicating better optical property with increasing Cr concentration. The I_{UV}/I_{vis} value depends on the competition of luminescence centre involving ultraviolet and visible light, the augment of I_{UV}/I_{vis} value indicate that the luminescence efficiency is enhanced, which reveals that Cr doping in ZnO could improve the exciton recombination probability.

4.1.6 Raman Analysis

Raman spectra of 500 °C sintered $Zn_{0.99}Cr_{0.01}O$, $Zn_{0.95}Cr_{0.05}O$, $Zn_{0.91}Cr_{0.09}O$ and 500 °C & 800°C sintered $Zn_{0.91}Cr_{0.09}O$ are presented in Figure 4.19 and Figure 4.20. The spectra shown in Figure 4.19 reveal all the standard phonon modes corresponding to bulk ZnO ceramic [16 - 18]. However, for all the doped samples there is a slight shift towards the low-frequency side, which depends on the residual stress, structural disorder and crystal defect in the samples. The vibration mode at 438 cm^{-1} is ascribed as E_2 (high) phonon mode, which is the typical Raman peak of ZnO bulk, has been seen to be present in all the samples. The tetrahedral sites in the wurtzite structure of ZnO are occupied by Zn ions which generate new crystalline lattice defects when substituted by ions of magnetic dopants [19]. For ZnO, Raman peak observed in between 570 and 590 cm^{-1} is assigned to A_1(LO) mode and is normally considered to be associated with structural disorders, such as oxygen vacancy, Zn interstitial and their combination, due to the strong dependence on the oxygen stoichiometry [20, 21]. Such a peak is located at 553 cm^{-1} which is quite narrow and has relatively high intensity for all the samples except for the 1% Cr doped sample. In Figure 4.19, additional Raman peaks are observed at 294, 334, 351, 529, 614 cm^{-1}, which are all identified as peaks corresponding to the vibration modes of Cr_2O_3 secondary phase in doped ZnO. It is noted that the defect induced peak of ZnO has been red-shifted and merged with the A_{1g} vibration peak of Cr_2O_3 at 553 cm^{-1} for the three samples of $Zn_{0.95}Cr_{0.05}O$ & $Zn_{0.91}Cr_{0.09}O$ sintered at 500 °C and

$Zn_{0.91}Cr_{0.09}O$ sintered at 800 °C. It is also noted that all the prominent Raman peaks corresponding to CrO_2 vibration modes; E_g (462 cm^{-1}), A_{1g} (580 cm^{-1}), B_{2g} (674 cm^{-1}) and B_{1g} (693 cm^{-1}), are appearing in the spectra of these three samples. Particularly, for $Zn_{0.91}Cr_{0.09}O$ sintered at 500 °C temperatures, the B_{2g} and B_{1g} peaks of CrO_2 vibration modes are merged to become a broader peak.

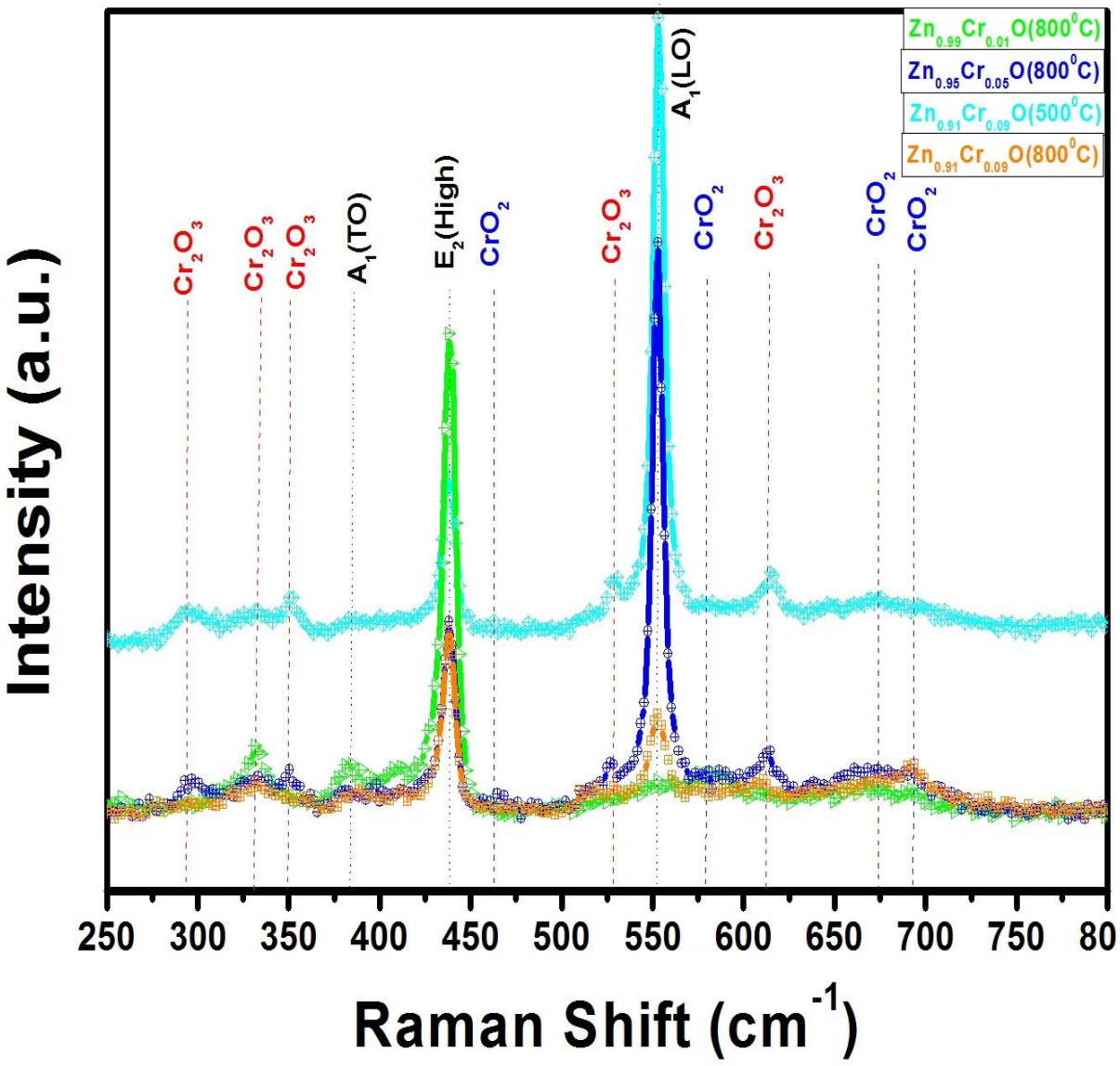

Figure 4.19 Raman spectra of $Zn_{1-x}Cr_xO$ sintered at 500 °C and 800 °C

It is further noticed that for the 1% Cr doped ZnO sample sintered at 800 °C (Figure 4.20), the defect induced peak is almost absent, whereas the intensity of the E_2 (high) characteristic

Raman peak is quite high. Similar observation is also noted for 1% Cr doped ZnO sintered at 500 °C (not shown). On the other hand, the integrated intensity ratio of A_1 (LO) mode to E_2 (High) mode [I_A/I_E] increase both for the 5% and 9% Cr doped ZnO samples sintered at 500 °C.

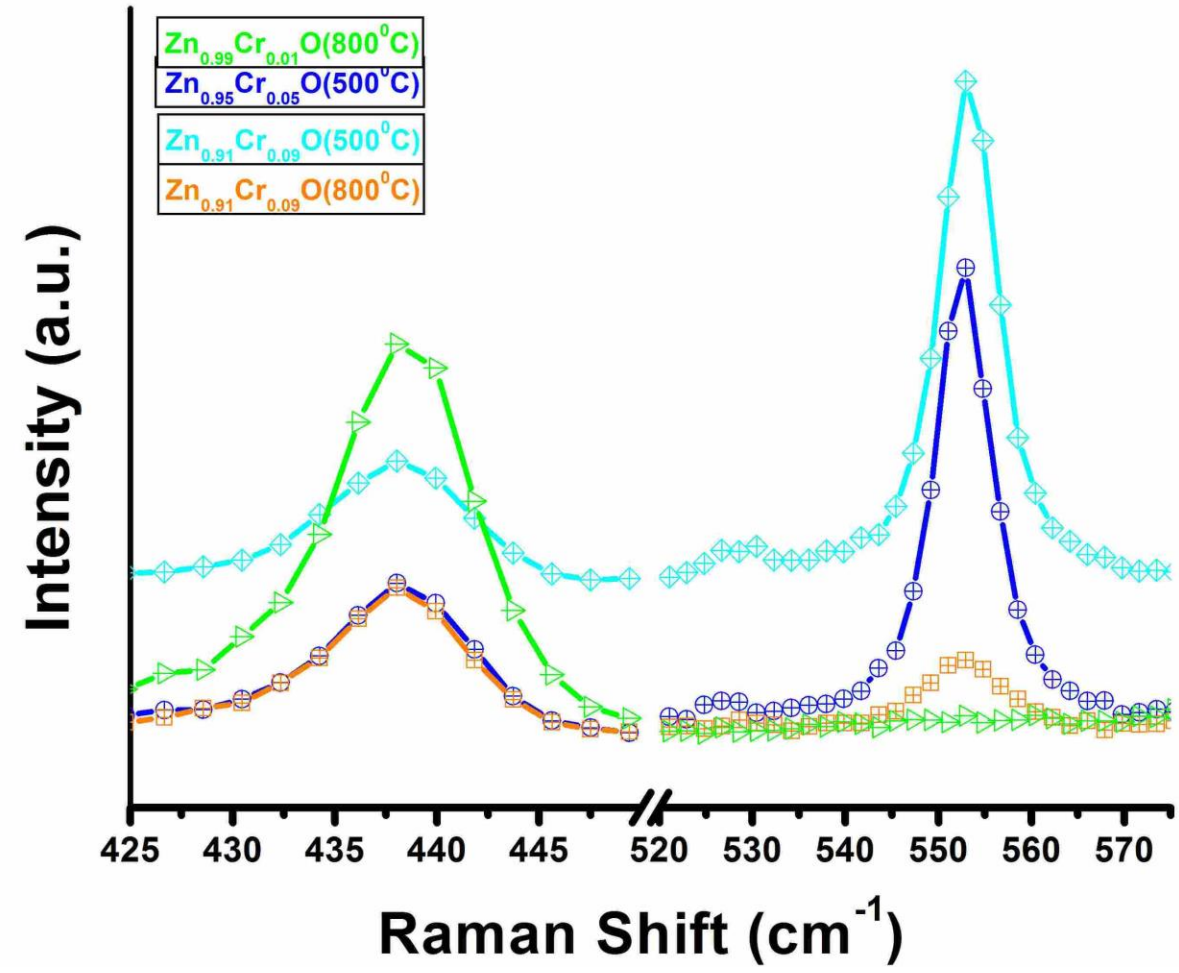

Figure 4.20 Broad Raman spectra of $Zn_{1-x}Cr_xO$ from 425 - 575 cm^{-1}.

The narrow and high intensity nature of the defect mode peak indicates the presence of oxygen vacancy in these two samples. In the 9% Cr doped ZnO samples; the I_A/I_E ratio has been reduced. It is not possible here to estimate the relative content of CrO_2 from the intensity ratio between CrO_2 and Cr_2O_3 peaks, as surface reactions like $2CrO_2 \rightarrow Cr_2O_3 + 1/2O_2$ often

occur which changes the final composition at the surface of the specimen [22]. It appears that with the increment of Cr content, the host lattice defects in ZnO matrix are activated. Cr^{3+} ions replacing Zn^{2+} ions could make more carriers than intrinsic activated donor defects (Zn_i, V_O) by isovalent doping. In fact, the increase in $[I_A/I_E]$ in $Zn_{1-x}Cr_xO$ indicates the creation of carriers with Cr incorporation. It is reported that [23] the major characteristic is universal to all of the models describing ferromagnetism in DMS is the strong electronic coupling between the magnetic ions and charge carriers created at the Fermi level.

4.1.7 Electron Spin Resonance (ESR) Analysis

The $Zn_{1-x}Cr_xO$ samples of all compositions were subjected to electron spin resonance (ESR) characterization at room temperature and the recorded spectra are presented in Figure 4.21. 1 at. % Cr doped ZnO samples sintered at 500 °C and 800 °C did not show any ESR signal, hence are not included in the figure 4.21. These two samples are seen to exhibit strong diamagnetic behaviour at room temperature (M-H plot in Figure 4.22 and Figure 4.23). ESR spectra of other four doped samples have a similar line shape, with the centre of resonance of $Zn_{0.95}Cr_{0.05}O$ sample sintered at 500 °C showing a shift towards lower field due to a possible internal field. The resonant signal corresponding to an effective g-value of 1.97 for the samples, may be attributed to the typical exchange coupled Cr^{3+} ion pairs [24, 25], concluding that trivalent states are dominant if the chromium concentration significantly exceeded the concentration of shallow donors in the system. The two 500 °C sintered samples of $Zn_{0.95}Cr_{0.05}O$ and $Zn_{0.91}Cr_{0.09}O$ have very broad signals with peak-to-peak line width of 431 and 564 G respectively. The broad signal is attributed to ferromagnetic resonance, arising from the secondary phases of Cr oxides and their inhomogeneous arrangement inside the system [24 - 27]. The broadening of the signal is an indicative of magnetic inhomogeneity of

the sample, whereas signals appearing in higher field regions points toward the existence of impurity phases in the samples. Samples of $Zn_{0.95}Cr_{0.05}O$ and $Zn_{0.91}Cr_{0.09}O$ sintered at 800 °C exhibits sharp resonance signals with improved magnetic homogeneity, with line width of 221 Oe respectively. These two samples show paramagnetic and antiferromagnetic behaviours respectively (Figure 4.21). Tentatively it can be suggested that Cr^{3+} is localized in the octahedral site and correspond not only to the Cr^{3+} ions observed in the compound, but also to an unpaired electron trapped at an oxygen vacancy site. It is possible that the broad line of the Cr^{3+} ions overlap with the resonance line of an unpaired electron trapped on an oxygen vacancy site.

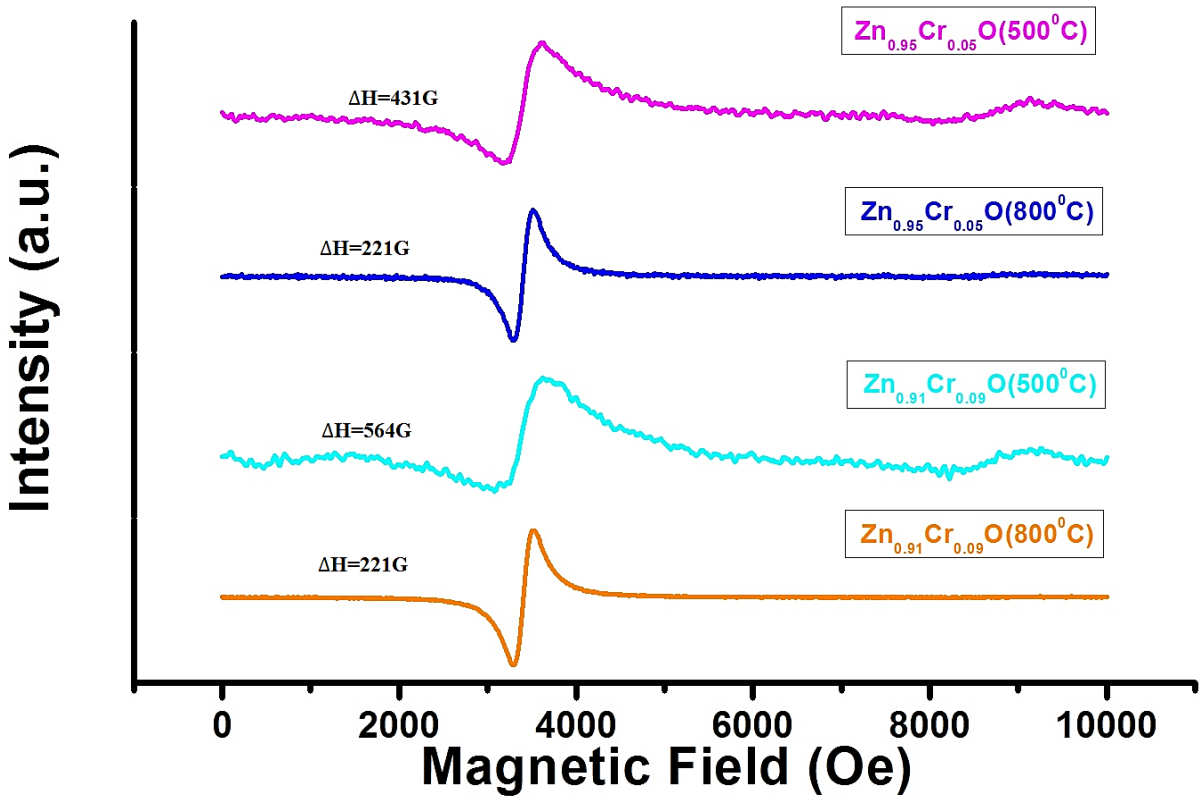

Figure 4.21 Electron spin resonance spectra of $Zn_{1-x}Cr_xO$, x=0.05 sintered at 500 °C and 800 °C and x= 0.09 sintered at 500 °C and 800 °C

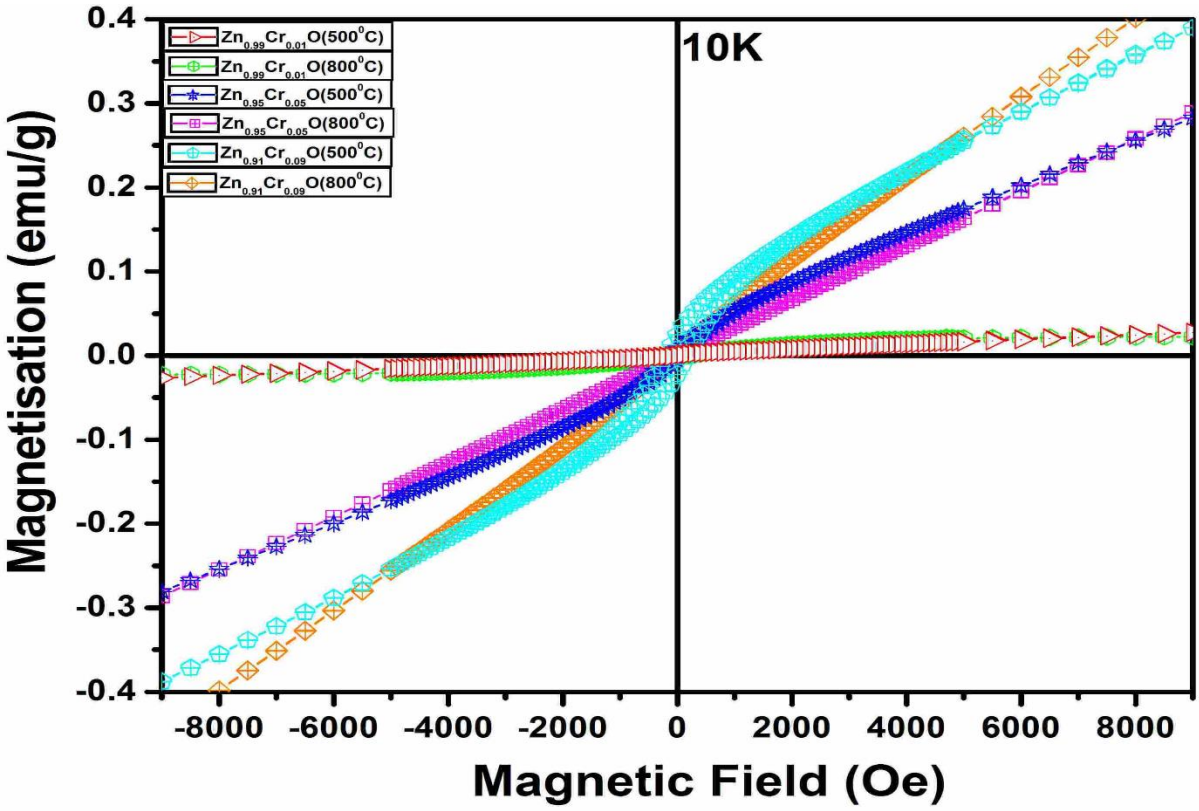

Figure 4.22 M~H curves of $Zn_{1-x}Cr_xO$ ($0.01 \leq x \leq 0.09$) at T = 10 K

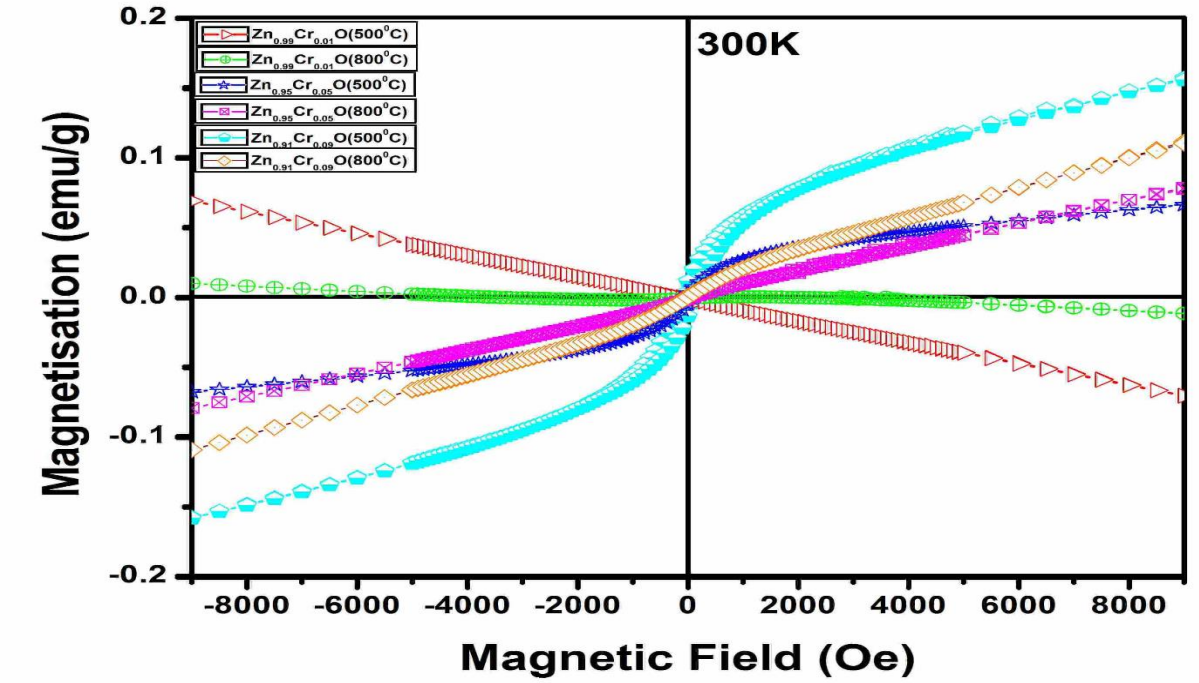

Figure 4.23 M~H curves of $Zn_{1-x}Cr_xO$ ($0.01 \leq x \leq 0.09$) at T = 300 K

Cr doping effect on the magnetic property of ZnO in our experiment has been presented in the M-H plot of Figure 4.22 and Figure 4.23. The magnetic field dependent magnetization at 10K shows antiferromagnetic nature for all the samples as shown in Figure 4.22. As it is reported that the Neel transition temperature of Cr_2O_3 is 309 K, at low temperature, AFM ordering is pronounced and therefore, all the samples shows AFM behaviour. However, at room temperature (300K), magnetic field dependent magnetization study for $Zn_{0.99}Cr_{0.01}O$ sintered at 500 °C and 800 °C show diamagnetic behaviour Figure 4.23. It is well known that when present in near proximity, Cr-Cr interaction exhibit antiferromagnetic nature. In our case when dopant level is low and dopants are distributed randomly inside the host semiconductors, the distance between the Cr ions is usually very large. Hence, the possibility of exchange interaction between Cr-Cr ions is almost negligible and the diamagnetic behaviour of ZnO is pronounced. This diamagnetic behaviour of $Zn_{0.99}Cr_{0.01}O$ is changed when Cr concentration in ZnO is increased to 5 at. % and 9 at. % level. $Zn_{0.95}Cr_{0.05}O$ and $Zn_{0.91}Cr_{0.09}O$ samples sintered at 500 °C shows ferromagnetic behaviour at room temperature. This may be due to the co-existence of a higher percentage of Cr_2O_3 phase and a lower percentage of CrO_2 phase in them. As widely observed, the magnetic behaviour of typical II-VI DMS materials has been due to the indirect sp-d interactions between the transition metal (TM) atoms, which could either be due to double-exchange (DE) or super-exchange (SE) interactions. While the former is a FM process, the later can be either FM or AFM for TMs with less than half filled d-shell [30]. It is presumed that presence of Cr in both 3+ and 4+ valence states inside the systems increases the long range exchange interaction and is responsible for the ferromagnetic behaviour. Usually higher magnetic moment is ascribed to an increasing occurrence of antiferromagnetic coupling between neighbouring magnetic ions due to super exchange interaction [31]. Favourable ferromagnetic super exchange between

Cr^{3+} may take place when a majority p-electron is transferred, increasing the spin and lowering the ground state energy in accordance with Hund's rule [32, 33]. Therefore, we conclude that super exchange interactions for higher dopant concentration are the cause of room temperature ferromagnetism for 5 at. % and 9 at. % Cr doped ZnO samples sintered at 500 °C.

On the other hand, the 800 °C sintered $Zn_{0.95}Cr_{0.05}O$ sample does not show ferromagnetism because of the unstable phase CrO_2 decomposing to stable Cr_2O_3 phase facilitated at higher temperature [22], which is evident in the XRD pattern of Figure 4.12. Due to the inhomogeneous arrangement of grains and distribution of Cr ions in the compound, antiferromagnetic behaviour is observed for this sample.

The antiferromagnetic ordering is also confirmed from the temperature dependent magnetization curve shown in Figure 4.24. The room temperature diamagnetic behaviour is evident both for the 500 °C and 800 °C sintered $Zn_{0.99}Cr_{0.01}O$ samples, where at lower temperature the samples show positive value of magnetisation. As seen clearly in the figure, both FC and ZFC curves diverge from each other below room temperature; but not saturated by lowering the temperature. Steady increase at low temperature, is an indication of PM/AFM nature of the samples. The bifurcation of FC and ZFC increases with the increasing concentration of Cr in ZnO. A decrease in magnetization value at around 25~30 K in the 800 °C sintered specimen of $Zn_{0.95}Cr_{0.05}O$ and $Zn_{0.91}Cr_{0.09}O$ has been noticed. Such type of decrease in magnetization is attributed to the presence of Cr_2O_3 in the samples. As it is evident from the micro-Raman analysis that oxygen vacancies are abundant in the 800 °C sintered samples, at low temperature the oxygen vacancies are responsible to mediate super-exchange interaction between Cr-Cr ions to show reduced magnetic moment.

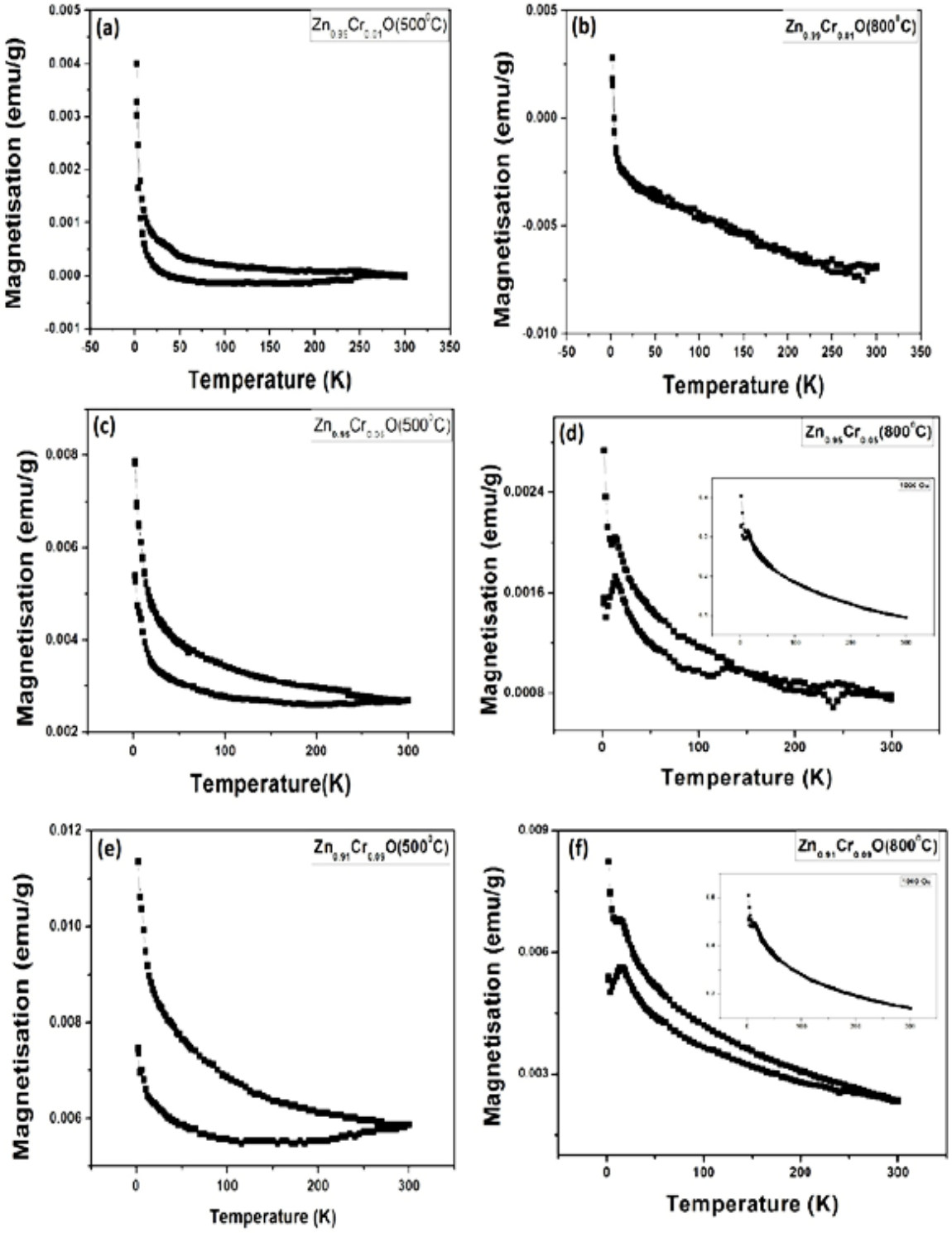

Figure 4.24: Magnetization vs. Temperature (M-T) curves of $Zn_{1-x}Cr_xO$ ($0.01 \leq x \leq 0.09$) sintered at 500 °C and 800 °C.

4.2 Conclusion

In summary, we report that from the Polycrystalline $Zn_{1-x}Cr_xO$ ($0.01 \leq x \leq 0.09$) samples synthesized by solid state reaction and from XRD patterns and Raman spectra, secondary phases have been detected with samples $x \geq 0.05$. Improved optical properties of the samples compared to undoped ZnO from Photoluminescence study. Low percentage of Cr doped samples showed diamagnetic behaviour while higher percentage doped samples ≥ 5% show ferromagnetic, paramagnetic behaviours depending upon sintering temperatures.

4.3 References

[1] Y.T.Prabhu, K.VenkateswaraRao, V. Sesha Sai Kumar, B.Siva Kumari, International Journal of Engineering and Advanced Technology, 2, (2013) 268-274.

[2] S. Senthilkumaar , K. Rajendran , S. Banerjee , T.K. Chini , V. Sengodan, Mate. Sci. Semi. Proces. 11 (2008) 6.

[3] S.Muthukumaran, R. Gopalakrishnan, Opt. Mat. 34 (2012) 1946.

[4] R.B. Bylsma, W.M.Becker, J. Kossut, U.Debaska, D.Yoder-Short, Phys.Rev. B (1986) 8207.

[5] F. Xu, Z.Y. Yuan, G.H. Du, T.Z. Ren, C. Volcke, P. Thiry, B.L. Su, J. Non-Cryst. Solids 352 (2006) 2569.

[6] C. Li, G. Fang, Q. Fu, F. Su, G. Li, X.Wu, X. Zhao, J. Cryst. Growth 292 (2006) 19.

[7] Y. Feng, Y. Zhou, Y. Liu, G. Zhang, X. Zhang, J. Lumin. 239 (2004) 119.

[8] V.A. Nikitenko, M.M. Malov, P.G. Pasko, V.D. Chernuj, J. Appl. Spectrosc. 21 (1974) 835.

[9] K. Vanheusden, W.L. Warren, C.H. Seager, D.R. Tallant, J.A. Voigt, B.E. Gnade, J. Appl. Phys. 79 (2006) 7983.

[10] Y. Sun, N.G. Ndifor-Angwafor, D.J. Riley, M.N.R. Ashfold, Chem. Phys. Lett., 431 (2006) 352.

[11] L.Wu, Y.Wu, X. Pan, F. Kong, Opt. Mater. 28 (2006) 418.

[12] I. Satoh, T. Kobayashi, Appl. Surf. Sci. 216 (2003) 603.

[13] K. Sato, H. Katayama-Yoshida, Physica B 308–310 (2001) 904.

[14] H. Liu, X. Zhang, L. Li, Y.X. Wang, K.H. Gao, Z.Q. Li, R.K. Zheng, S.P. Ringer, B. Zhang, X.X. Zhang, Appl. Phys. Lett. 91 (2007) 072511.

[15] Y.W. Chen, Y.C. Liu, S.X. Lu, C.S. Xu, C.L. Shao, C. Wang, J.Y. Zhang, Y.M. Lu, D.Z. Shen, X.W. Fan, J. Chem. Phys. 123 (2005) 134701.

[16] J. M. Calleja, M. Cardona, Phys. Rev. B 16 (1977) 3753.

[17] N. Ashkenov, B.N. Mbenkum, C. Bundesmann, V. Riede, M. Lorenz, D. Spemann, E.M. Kaidashev, A. Kasic, M. Schubert, M. Grundmann, J. Appl. Phys. 93 (2003) 126.

[18] J.F. Scott, Phys. Rev. B 2(1970) 1209.

[19] K. Samanta, P. Bhattacharya, R.S. Katiyar, Phys. Rev. B 73 (2006) 245213.

[20] R. Cusco, E.A. Llado, et al., Phys. Rev. B 75 (2007) 165202.

[21] S.H. Jeong, J.K. Kim, B.T. Lee, J. Phys. D: Appl. Phys. 36 (2003) 2017.

[22] Y. Chen, K. Ding, L. Yang, B. Xie, F. Song, J. Wan, G. Wang, M. Han, Appl. Phys. Lett. 92 (2008) 173112.

[23] K.R. Kittilstved, W.K. Liu, D.R. Gamelin, Nat. Mater. **5** (2006) 291.

[24] J. J. Kerbs, G. H. Strauss, Phys. Rev. B 15 (1977) 17-22

[25] G. Krishnaiah, N.M. Rao, B.K. Reddy, D.R. Reddy, T.M. Babu, S. Sambasivam, P.S. Reddy, Phys. Lett. A 372 (2008) 6429-6433.

[26] J. Hays, K.M. Reddy, N.Y. Graces, M.H. Engelhard, V. Shutthanandan, M. Luo, C. Xu, N.C. Giles, C. Wang, S. Thevuthasan, A. Punnoose, J. Phys. Conden. Matter 19 (2007) 266203.

[27] J. Hays, A. Punnoose, R. Baldner, M.H. Engelhard, J. Peloquin, K.M. Reddy, Phys. Rev. B 72 (2005) 075203.

[28] P. Sati, R. Hayn, R. Kuzian, S. Regnier, S. Schafer, A. Stepanov, C. Morhain, C. Deparis, M. Laugt, M. Goiran and Z. Golacki, Phys. Rev. Lett. 96 (2006) 17203.

[29] K. Srinivas, S.M. Rao, P.V. Reddy, J. Nanoparticle Research 13 (2011) 817-837.

[30] R.D. McNorton, J.M. MacLaren, J. Phys. Condens. Matter. 21 (2009) 445803.

[31] K. Rode, A. Anane, R. Mattana, J.P. Contour, O. Durand, R. Lebourgeois, J. Appl. Phys. 93 (2003) 7676.

[32] J. Kanamori, Prog. Theor. Phys. 30 (1963) 275.

[33] L.B. Duan, X.R. Zhao, J.M. Liu, T. Wang, G.H. Rao, Appl. Phys. A 99 (2010) 679-683.

CHAPTER FIVE

CONCLUSION AND FUTURE WORK

5.1 Conclusions

In order to produce semiconductor based spintronic devices, it is important to improve existing functionality and developing new functionality like the spin LED, spin transistors etc. To attain this type of functionality it is expedient that the DMS material should be ferromagnetic at just above room temperature or at room temperature. It is also important that the ferromagnetism of the DMS material should be intrinsic and single phase that is to say the ferromagnetic behaviour is not as result of secondary phases or precipitates present in the material.

We have presented the structure and spin dynamics of transition metal doped ZnO focusing on $Zn_{1-x}Cr_xO$ (x= 0.01, 0.05, 0.09), using Cr as the dopant material. Cr doping and the sintering effect on the optical and magnetic behaviour of ZnO has been investigated. Creation of chromium secondary phases like Cr_2O_3 and CrO_2 in the samples with dopant level ≥ 0.05 has been established through the XRD and Raman studies. PL study performed on the samples indicates better optical property due to Cr doping. UV-Vis study shows decrease in band gap with increasing dopant concentration for both the sintering temperature. It is presumed that the Cr–O–Cr super exchange interaction is the controlling factor for the typical magnetic behaviour observed in the $Zn_{1-x}Cr_xO$ ($0 \leq x \leq 0.09$), consequently, leading to an enhancement of FM ordering with the increase in Cr content. ESR and XRD studies support the +3 valence state of Cr in ZnO matrix. It is believed that Cr doping as well as the slow step sintering schedule adopted during sample synthesis has created suitable environment for

enhanced magnetic and optical property in ZnO. The sintering process also seen to affect magnetic homogeneity in the doped system.

5.2 Future Work

Polycrystalline sample of $Zn_{1-x}Cr_xO$ was focussed on this study and having successfully studied Cr doping and the sintering effect on the optical and magnetic behaviour of ZnO, we will be studying other transition metals such as Co, Fe, Ni and Mn as well as rare earth elements like Gd, Sm, Eu, Dy doped ZnO systems for our future work. This will enable us understand more on the optical properties and magnetic behaviour of rare earth metal/TM doped ZnO systems of DMS materials.

Appendix

A.0 Publications

1. Effect of Cr doping and slow step sintering process on the optical and magnetic properties of $Zn_{1-x}Cr_xO$ ($0.01 \leq x \leq 0.09$). (Revised manuscript submitted to Journal of Materials Chemistry and Physics).